LOCKHEED MISSILES AND SPACE COMPANY
A GROUP DIVISION OF LOCKHEED AIRCRAFT CORPORATION
Sunnyvale, California

MANUFACTURING RESEARCH INVESTIGATION
FINAL REPORT

NON-DESTRUCTIVE TESTING,
INSPECTION - PYROLYTIC GRAPHITE

MRI 228.05
12C SV60

6 June 1962

Prepared by: _____
L. S. McCollum, Manufacturing Research Engineer, Seni
Metals Development Group

Approved by: _____
F. C. Hoffman, Supervisor
Metals Development Group

Approved by: _____
George Irving, Manager
Manufacturing Development

ABSTRACT

NON-DESTRUCTIVE TESTING, INSPECTION - PYROLYTIC GRAPHITE

SUMMARY:

This investigation objectively extends certain non-destructive tests methods to include pyrolytic graphite as one of the newer materials that can be readily examined by these methods. Refinement of previously standardized technique and adaptation of evaluation parameters, peculiar to the material, were important facets in establishing predominant characteristics in individual plates, shapes, and other test specimens.

In this report, each of the methods used are described and basic concepts, related to the apparatus and technique involved, are reviewed. Representative studies on some specimens are then discussed as illustrations.

CONCLUSIONS:

The science of non-destructive testing can be successfully applied toward determination of several characteristics found in pyrolytic graphite. With these methods it was possible to detect external and internal flaws or imperfections, microstructures, parallelism of layer planes, internal stresses, and dimensions, such as thicknesses of supplied materials.

The capability developed during this program has brought forth several conclusions. These are defined in the following statements:

1. Penetrant inspection is a rapid method of determining connected surface structure discontinuities.

2. The sonic method is not a reliable technique for locating internal flaws. It can be used, however, to confirm such areas when located by other methods.

3. Ultrasonic examination is the optimum method for determination of internal discontinuities and for use on a production line basis.

4. Radiography is the optimum method for determination of nodule characteristics and micro-structure.

5. The X-ray diffraction method is the optimum for evaluating internal stresses in both tensile and compression directions.

6. The Eddy-Current method is the optimum for determination of parallelism of layer planes.

7. Thermal gradient methods, for use on pyrolytic graphite examinations, are not yet sufficiently developed. Results appear encouraging but no conclusions are presently drawn.

NON-DESTRUCTIVE TESTING, INSPECTION - PYROLYTIC GRAPHITE

8. Reliable and accurate analyses of internal stresses was a substantial aid in improving the quality of pyrolytic graphite as produced by the manufacturers.

9. Materials received from manufacturers toward the latter stages of this program were much superior in quality, and more uniform than earlier shipments.

RECOMMENDATIONS:

These are reserved for the Value and Production Engineering Department, Organization 81-41. The cooperation and assistance of R. M. Parker, 81-41 in this investigation is gratefully recognized.

NON-DESTRUCTIVE TESTING, INSPECTION - PYROLYTIC GRAPHITE

Table of Contents

NON-DESTRUCTIVE TESTING, INSPECTION - PYROLYTIC GRAPHITE

1. OBJECT:

This investigation was conducted at the request of Value and Production Engineering Department, Organization 81-41. The purpose was to develop non-destructive test methods and techniques capable of determining pyrolytic graphite material conformance to design requirements.

2. INTRODUCTION:

In recent years the use of non-destructive testing methods and techniques for evaluation of materials, components and assemblies has grown to a great extent. Its growth has been similar to and parallels that of mass production methods and automation of industrial processes. The advent of critical and highly expensive materials has placed additional demands upon non-destructive testing of such magnitude that new and improved methods must be continually developed.

Pyrolytic graphite is a new material of unusual structure and its adaptation for use in the aerospace industry requires careful study of characteristics and physical properties. It is an extremely expensive material, presently in limited supply. Non-destructive testing, to determine it qualities, is therefore mandatory, and the results correlated with test pieces that must be destructively evaluated for necessary comparisons.

3. PROCEDURE:

3.1 Other responsible organizations were involved in this investigation and liaison was maintained with representatives from each. These included Organization 81-41, Value and Production Engineering, Organization 70-64, Quality Assurance - Receiving; Organization 81-90, Re-Entry Systems; Organization 70-21, Materials and Process Laboratories; Organization 71-22 N.D.T. Group; Organization 58-11, Communications and Controls; and Organization 53-35, Chemistry and Plastics. The latter two were frequently contacted for specialized tests and discussion comments.

3.2 Pyrolytic graphite is a highly refined form of graphite with properties significantly different from ordinary commercial types. The most interesting of these qualities are: high density, anistropic thermal and electrical conductivity properties, and impermeability to gases. Its extra ordinary resistance to non-oxidizing extreme temperature conditions is of prime importance.

The suitability of this material for its intended use in the field of missiles required exhaustive study and literally hundreds of tests to determine its properties for anticipated use conditions. At the beginning of this investigation, certain fundamental data had previously been established but many crucial measurements were yet to be accomplished.

NON-DESTRUCTIVE TESTING, INSPECTION - PYROLYTIC GRAPHITE

As stated, the structure of pyrolytic graphite is unique and unusual. This made it necessary to consider carefully the non-destructive test methods which would most likely prove practical; less promising methods were also investigated for comparison purposes. Further, some attempt was directed toward the development of methods peculiarly adaptable to pyrolytic graphite alone.

3.3 By definition, the science of non-destructive testing includes all possible methods of detection or measurement of the properties or performance capabilities of materials, parts, assemblies, structures or systems, which do not impair their serviceability. Such measurements are usually indirect; the property measured by test must be proven by other means, such as destructive tests or service experience. The detection and evaluation of discontinuities and defects, are the normal functions of non-destructive tests; as well as the determination of material characteristics in the absence of faults or defects.

Direct measurements such as commonly used in precision gauging, for example, are not ordinarily considered to be in the area of non-destructive testing. Gauging by indirect means, however, as by X-ray absorption or ultrasonic resonance within the test material is a typical non-destructive test.

In line with this definition and example a procedural approach to non-destructive testing pyrolytic graphite was established. The methods most commonly referred to in this report are shown below. With the exception of the thermal gradient or infra-red method all equipment and instruments required are standard.

1. Fluorescent penetrant.
2. Sonic.
3. Ultrasonic (pulse and resonance).
4. Radiographic.
5. Eddy-current.
6. X-ray diffraction.
7. Thermal gradient

Information obtained by applying these methods to test specimens and later to full size shapes allowed evaluations to be readily made. By these means it was possible to locate faults and defects, both obvious and minute in character. Sub-standard material was detected by internal cracks, inclusions or laminations as disclosed by one or more of the test methods.

More critical examinations with X-ray diffraction and to some extent eddy-current apparatus permitted highly specialized determinations. Such data dealt with type of microstructure, electrical conductivity, layer parallelism indications and degree of internal stresses.

4. RESULTS:

4.1 The achieved results appear adequate for reliable conclusions on the feasibility of non-destructive test methods for evaluation of this material. Those used during the program are documented by literature and illustrated in this report. Individual performance records of some pyrolytic graphite samples and shapes are submitted.

5. DISCUSSION OF RESULTS:

5.1 This report will develop discussions along several lines, each related either as background information or data concerning the characteristics of pyrolytic graphite specimens under test. In a broad sense, discussion items occur in the following order:

1. Pyrolytic graphite - its manufacture and structure.
2. Description of non-destructive test methods and apparatus.
3. Performance information and data.

5.2 Pyrolytic graphite - its manufacture and structure.

5.2.1 The material being investigated is produced by gaseous decomposition of methane. This is accomplished by running the gas through a vacuum furnace at temperatures ranging between about 1900°and 2500°C. As the gas decomposes, carbon deposits in an orderly fashion, layer by layer, on a mandrel in the furnace. This mandrel is pre-shaped to a desired configuration, such as a flat plate, semi-hemisphere or any other convenient or required design. Ordinary structural graphite is used for mandrel purposes. Its coefficient of expansion-contraction being greater than the pyrolytic graphite allows it to be withdrawn when a run is completed and the system cooled down.

A schematic flow sheet of the process accompanies this report. See Figure 1.

Pyrolytic graphite is shown to be an anistropic material of hexagonal crystalline configuration. The cone or fiber-like structure is highly oriented as may be expected by its deposition method of manufacture. Compared with commercial graphite which may reach an orientation ratio of 3 to 1 (that is, three crystals with their "c" axes oritented perpendicular to the surface for every one crystal oriented parallel to the surface), pyrolytic graphite may have orientation ratios as high as 100 or 1000 to 1.

NON-DESTRUCTIVE TESTING, INSPECTION - PYROLYTIC GRAPHITE

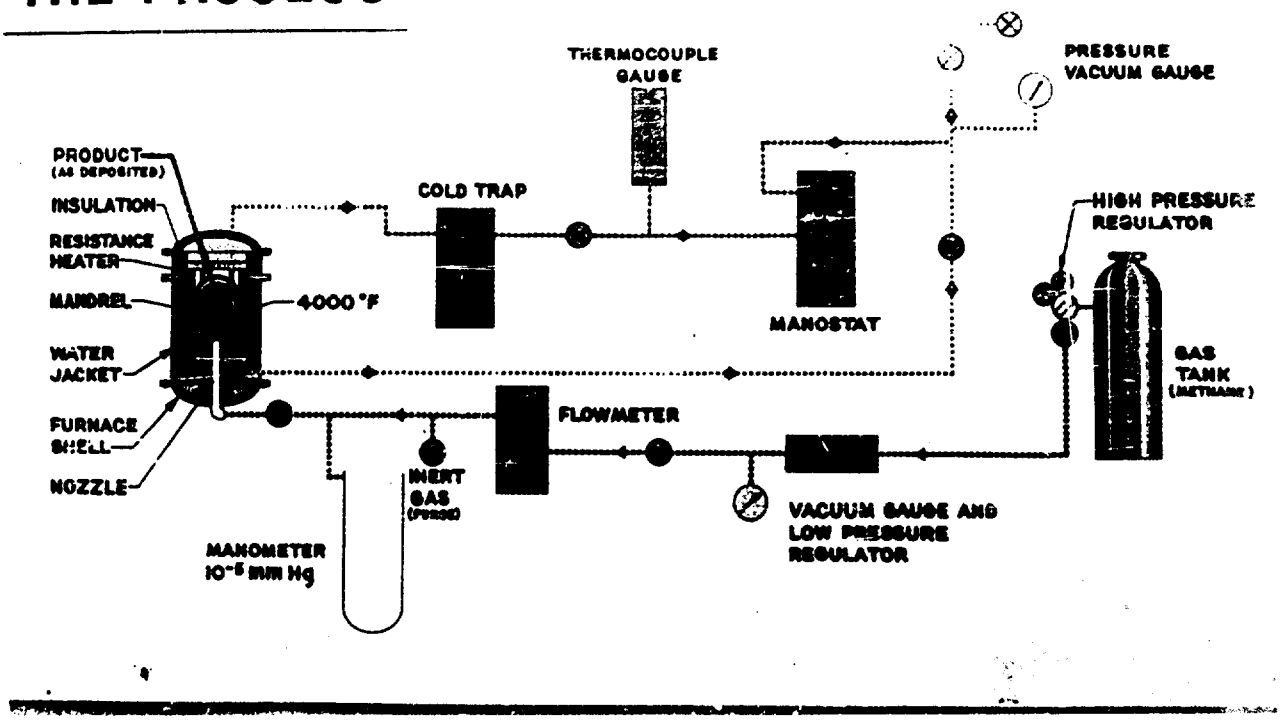

Figure 1

Schematic flow sheet for small scale production of Pyrolytic Graphite.

NON-DESTRUCTIVE TESTING, INSPECTION - PYROLYTIC GRAPHITE

In the presently intended use for pyrolytic graphite its attraction is principally derived from its thermal anistrophy, that is, its ability to conduct heat readily in one direction and block it in another. Theoretically, heat may be conducted, parallel to the surface, 50 to 1000 times faster than when conduction perpendicular to the surface is attempted. At the same time this material retains the high sublimation temperature common to other solid carbons, approximately 6900°F.

Graphite and pyrolytic graphite models are attached to this report. See Figure 2 and 3. Photomicrographs of typical pyrolytic structures are also attached. See Appendix A.

5.3 Non-destructive test methods and apparatus.

5.3.1 Fluorescent Penetrant Method - Visual examination and inspection of all specimens were generally the first order of determining type and quality of pyrolytic graphite specimens, parts or shape. A dimensional and alignment verification was an additional requirement at this initial stage of N-D testing.

In order to make surface defects easily detectable a fluorescent penetrant solution was used; either spraying the part or immersing it served to accentuate most surface imperfections.

After cleaning off the surplus liquid, a development process was used which caused surface defects to become more easily visible. For example, certain chemical substances fluoresce under ultraviolet light, so that a fine crack into which the liquid flowed would be easily visible under such light.

By this method, (MIL-I-6866, Type I) flaked areas on mandrel side surfaces were noted as well as sooty areas and miscellaneous surface inclusions. Particularly significant was the fact that "loose" nodules gave very clear indications at their periphery on the free surface side; such imperfections were evident on both machined and unmachined surfaces.

5.3.2 Ultrasonic Methods - In order to understand the behavior of ultrasonics in their applications to non-destructive testing one should be familiar with the origin of sound waves and their mode of travel. Sound is produced when a body vibrates. The pitch of its resultant note is determined by its frequency, i.e., the number of complete vibrations executed in one second, expressed in cycles per second. Since modern instruments permit vibrations in the order of millions per second, frequencies are ordinarily expressed in megacycles per second.

NON-DESTRUCTIVE TESTING, INSPECTION - PYROLYTIC GRAPHITE

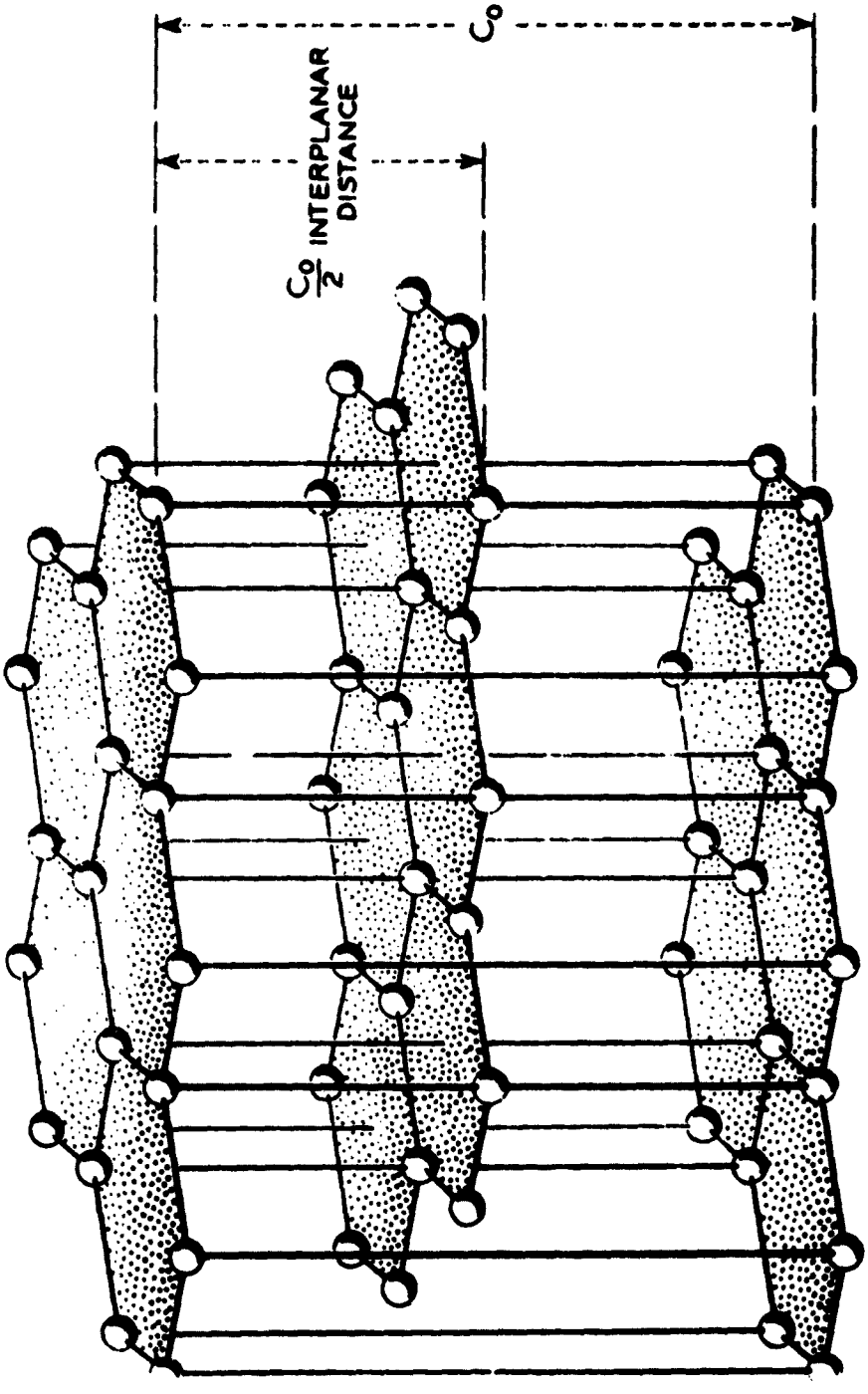

Figure 2

Structure of the most abundant form of graphite.

NON-DESTRUCTIVE TESTING, INSPECTION - PYROLYTIC GRAPHITE

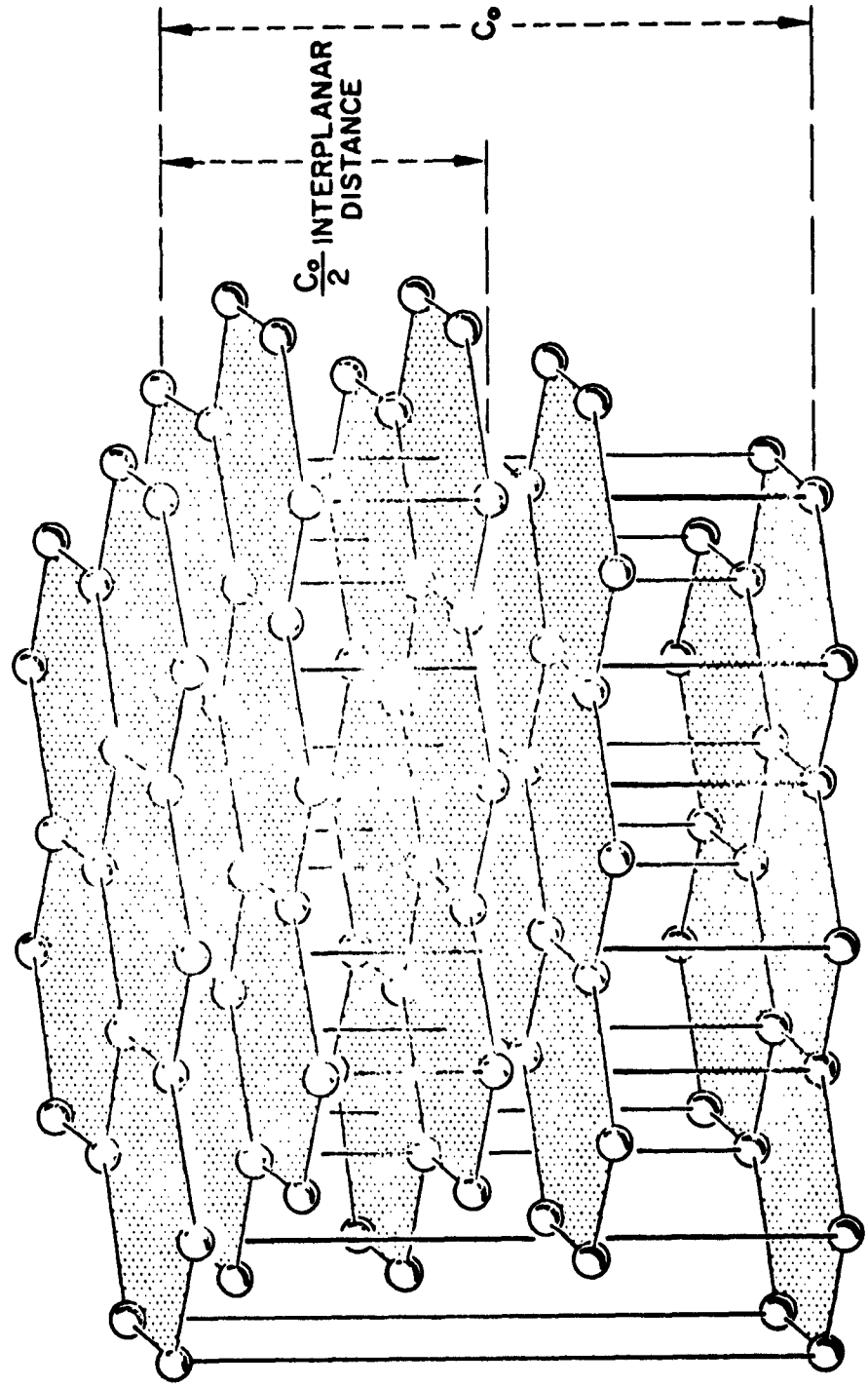

Figure 3

Proposed Pyrolytic Graphite Lattice. Increased density with slightly more random cell distribution than graphite shown in Figure 2.

NON-DESTRUCTIVE TESTING, INSPECTION - PYROLYTIC GRAPHITE

The main objects of testing by ultrasonic means are:

1. Flaw detection.
2. Thickness measurements.
3. Absorption measurements.

Determination of these features was achieved by two methods, namely the pulse technique and the resonance method.

With resonance methods a quartz crystal is excited by means of an oscillator at some frequency well below its fundamental resonance frequency while held on the surface of the specimen. This instrument is termed a Vidigage and was successfully used in the program to determine thicknesses of submitted specimens. Acoustic contact is maintained by means of suitable coupling devices or medium. Longitudinal waves from the crystal cause the sample to vibrate in the direction of its thickness. The frequency of the vibration of the crystal is varied until the sample resonates, i.e., oscillates with maximum intensity. This results in an increase in the amplitude of crystal vibrations as well as an increase in induced voltage. Resonance occurs at one of the natural frequencies of the specimen in its thickness direction and is in the order of exact half-wave lengths. Simple mathematicl calculations determine exact thicknesses. For example, assume the following term definitions:

F_n = Frequency
X_n = Wave Length
d = Thickness
n = Whole Number
c = Velocity of sound in the specimen

By formula calculations both thickness and frequency are determined, as below.

$d = n \times n/2$
$F_n = c/Xn = nc/d2$

The frequency range selected as most suitable was the 2-4 megacycle sweep. Higher ranges are more sensitive to layer imperfections, but for most pyrolytic graphite specimens, these yield excessive indications making evaluation difficult. Changing frequency ranges is accomplished by plug-in components and by spreading the harmonic pips further apart, recognition of particular harmonics is simplified.

The pulse echo method was developed originally from radar techniques. It can be used to achieve all three objectives mentioned above. Pulses of sound waves are transmitted at regular intervals through the medium and reflected back, either at a boundary or a defect, to the source. The position where the reflection occurs is located by

measuring the time taken for the return journey and multiplying half that quantity by the velocity of sound in the medium.

A simplified block diagram of the type apparatus used for this purpose is shown in Figure 4. Illustrations of results from sound and unsound specimens are shown in Figure 5.

The pulse echo equipment (Immerscope) was used to locate flaws whereas the depth and extent of such imperfections were defined by the resonance (Vidigage) method. Since the normal water immersion was not possible for pyrolytic graphite test models because of test tank limitations, contact crystals were employed for oscilloscope display. In this case, reflectoscope probes consisted of 5 and 10 megacycles crystals.

5.3.3 Radiography - In contrast to transistory images produced on the screen of fluoroscopic apparatus, radiography is concerned with recording internal features of objects revealed by passing penetrating radiation through the objects. The recording is achieved by using a photographic film to receive the X-ray images or shadowgraphs. The film has an image projected onto it for a given time - the exposure period - and is then processed by ordinary photographic procedure. The scheme for producing a radiograph, reduced to its simplest form, is shown in Figure 6.

The equipment used in this program is a Picker, 0-35kVp, beryllium window tube instrument. The film is Gevaert D-2 single emulsion; developed to 2.0 film density. Pentrameters and technique employed were in accordance with MIL I-6866B(2).

5.3.4 Eddy-Current Methods - The use of eddy-current techniques in measuring electrical conductivity has been well established. The extension of the technique to the detection and assessment of microstructure type parallelism and internal stresses in pyrolytic graphite was accomplished toward the latter part of this program.

Eddy-current testing is based upon electrical conductivity characteristics. Mathematics involved in analyzing the method become cumbersome but the qualitative aspects of the theory are not difficult to grasp. Thus, if a piece of electrical conductive material is placed in a field of an exciting coil (See Figure 7) it behaves as another coil with very low resistance with its begining connected to its end, that is, short circuited on itself. Alternating current flowing through the coil induces currents in any other coil linked with it, and consequently in this case with a pyrolytic graphite specimen, acting as a low resistance secondary coil. The induced current in the specimen flows in circulatory paths, and this feature accounts for the term "eddy-current".

NON-DESTRUCTIVE TESTING, INSPECTION - PYROLYTIC GRAPHITE

Under appropriate boundary conditions, the phase, direction and amplitude of the eddy-current at any point in the test piece can be computed from convenient formulas, provided dimensional data are known.

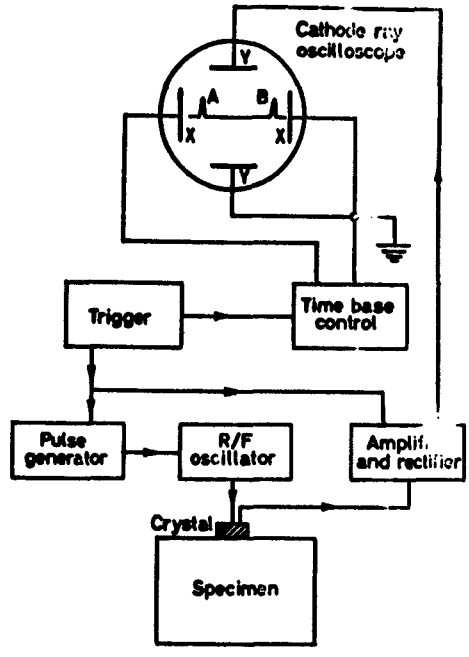

Figure 4

Simplified block diagram of the apparatus used for the pulse method of ultrasonic flaw detection.

NON-DESTRUCTIVE TESTING, INSPECTION - PYROLYTIC GRAPHITE

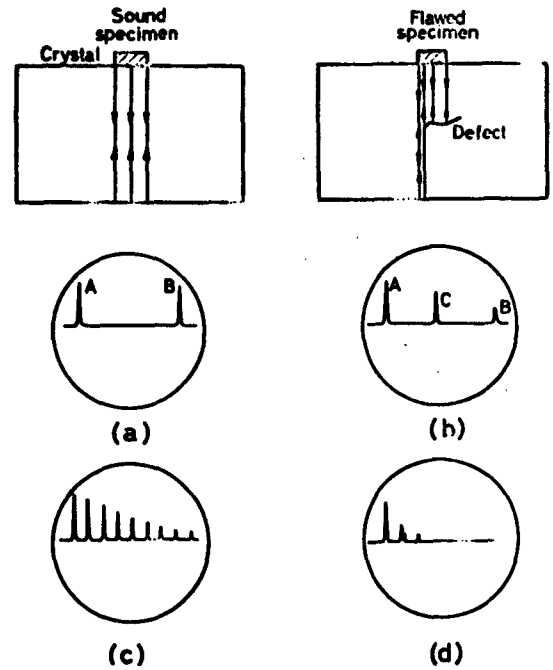

Figure 5

Typical indications of cathode ray oscilloscope with pulse technique of ultrasonic testing.

a. Sound specimen b. Flawed specimen
c. Sound specimen with low absorption coefficient
d. Sound specimen with high absorption coefficient

NON-DESTRUCTIVE TESTING, INSPECTION - PYROLYTIC GRAPHITE

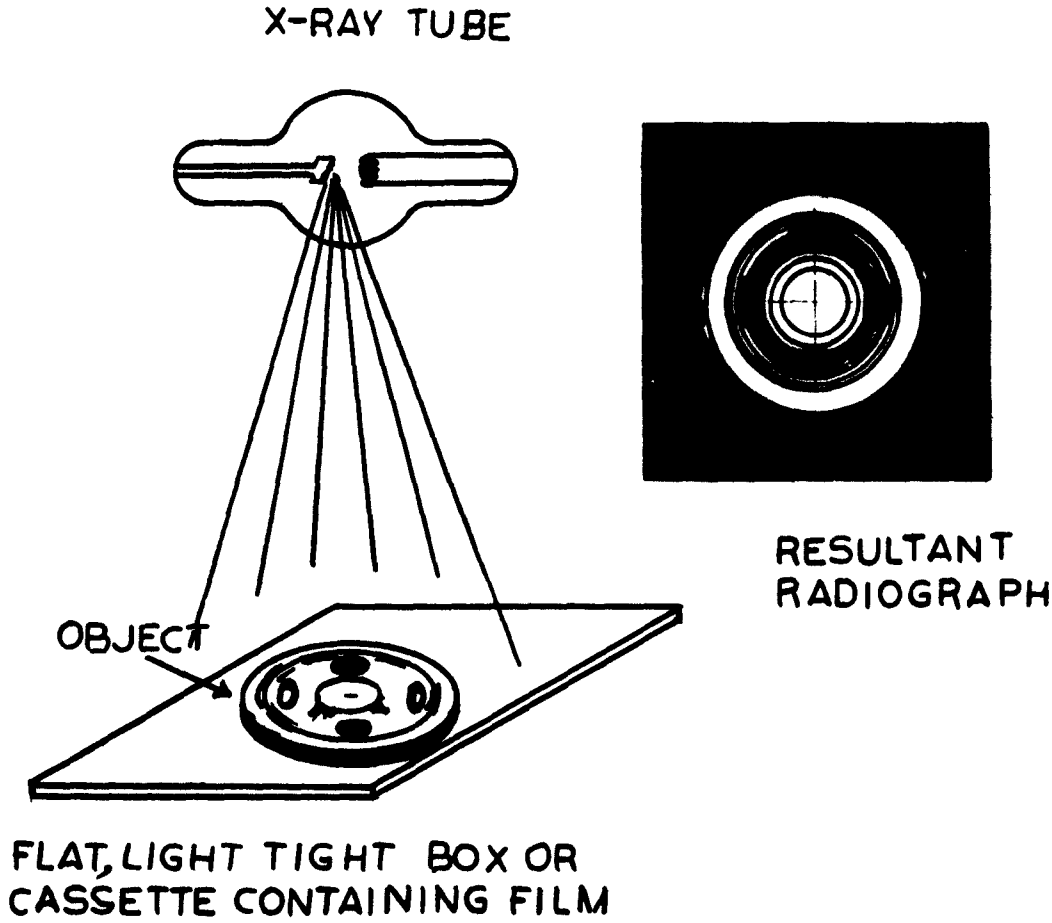

Figure 6

Simple illustration of X-ray reproduction.

NON-DESTRUCTIVE TESTING, INSPECTION - PYROLYTIC GRAPHITE

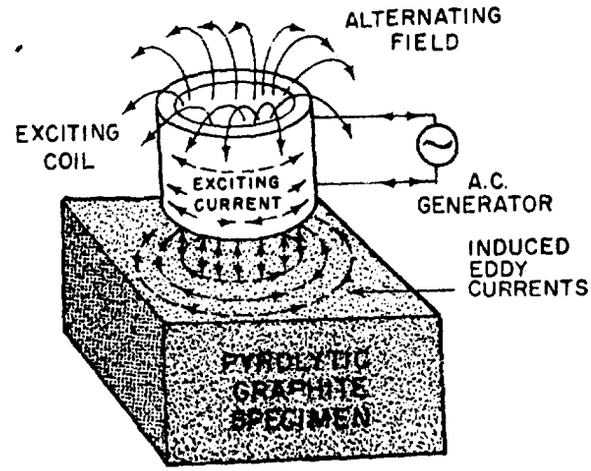

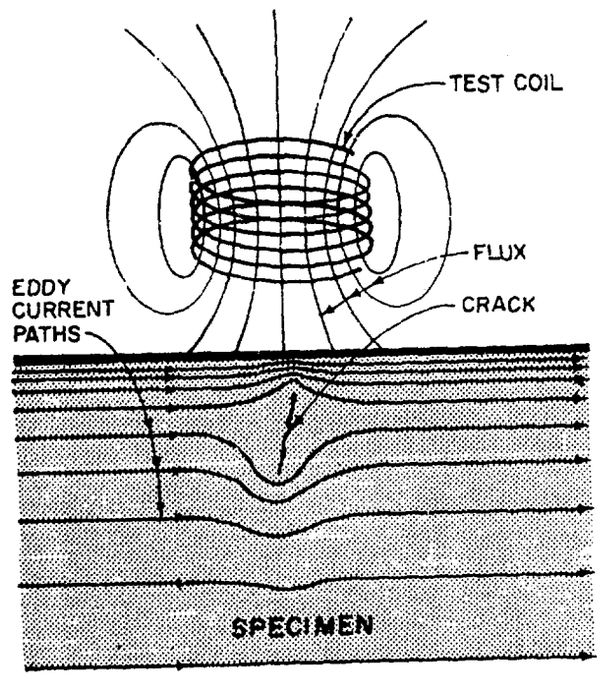

Figure 7

Eddy-Current Principle

NON-DESTRUCTIVE TESTING, INSPECTION - PYROLYTIC GRAPHITE

5.3.5 Stress Analysis by X-ray Diffraction - This method of non-destructive testing has proven invaluable in determining type and extent of internal stresses present in pyrolytic graphite.

In this method, a fine beam of monochromatic (single wave lengths) X-rays impinges upon and is diffracted by the specimen structure. Bragg's Law of Diffraction ($\lambda = 2d \sin \theta$) sets up geometrical requirements in terms of the perpendicular distance (d) between a given set of parallel atomic planes, the wave length (λ) of the incident monochromatic radiation, and the angle (θ) between the incident radiation and the atomic planes.

This law thus provides for the measurement of d dimension. The d spacing of crystallographic atomic planes in a stress-free body is constant for a given temperature and is determined by interatomic forces. When the specimen structure is distorted or elastically strained as in the case of residual stress, the d value changes as the interatomic forces and thus the spacing between atoms adjusts to accommodate the acting stress.

Bragg's Law is a simple representation of diffraction conditions. It is based on the idea of reflection X-rays from lattice planes rather than diffraction by lattice rows. The below sketch is intended to clarify the mechanics of this law.

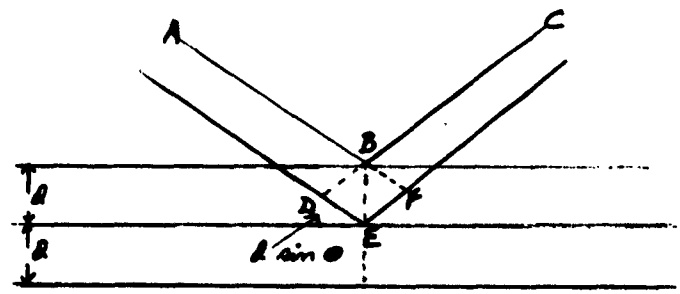

Figure 8

NON-DESTRUCTIVE TESTING, INSPECTION - PYROLYTIC GRAPHITE

Let AB be the primary X-ray beam of wave length λ , incident on a crystal; the planes, d, are at an angle $\measuredangle$ with the beam. A reflected beam BC will be formed by Huygens principle. There will be reinforcement by the beam from the next parallel lattice plane only when the path differences of DE + EF are equal to a whole number of wave lengths. This occurs when Bragg's Law is fulfilled; the diffracted waves from all lattice points of the crystal are in phase. The Debye-Scherrer ring (See Figure 9 and 10) results from this phenomenon. Principally, only the back reflection range applies and, therefore, a wave length of X-rays is necessary which forms an intense, strong Debye-Scherrer ring. The collimated beam of X-rays is passed through and at right angles to the photographic film. The beam strikes the specimen and is diffracted by atomic planes oriented such that conditions set by Braggs equation are satisfied. The diffracted radiation in the form of a cone with the incident radiation as its axis strikes the flat film forming an arc. Measurement of the radius of the arc along the film to specimen distance yields the data for calculation of the stress.

Internal stress is evident when misalignment of the Debye-Scherrer ring is observed. For example, one half of the X-ray film is covered while a first exposure is taken. After this exposure the camera and covering plate are turned 180° so that the unexposed part of the film takes the place of the previous exposure. This section is then filmed and the complete Debye-Scherrer ring examined for alignment. See Figure 9. The numerical value is obtained by line comparison from which the type and extent (psi) of internal stress is calculated. Appendix B contains mathematicl calculations relative to this method as prepared by R. Parker, Organization 81-41. Accurate line comparison is obtained by use of a modified, though fully equipped, densitometer.

5.3.6 Sonic Methods - Sonic testing was used frequently on pyrolytic graphite specimens and shapes. Primarily the purpose was to determine thicknesses only. An "audigage" instrument, equipped with dial gage and headphone sets, was the preferred equipment. The frequencies transmitted by means of a transducer are not immediately known but these produce audible signals as well as visual indications on the accessory meter. The instrument had been calibrated for use on several metals as well as on pyrolytic graphite.

Results were considered reliable for thickness measurements and gave, as well, indications of cracks by tone vibrations from established harmonics on identical thicknesses.

NON-DESTRUCTIVE TESTING, INSPECTION - PYROLYTIC GRAPHITE

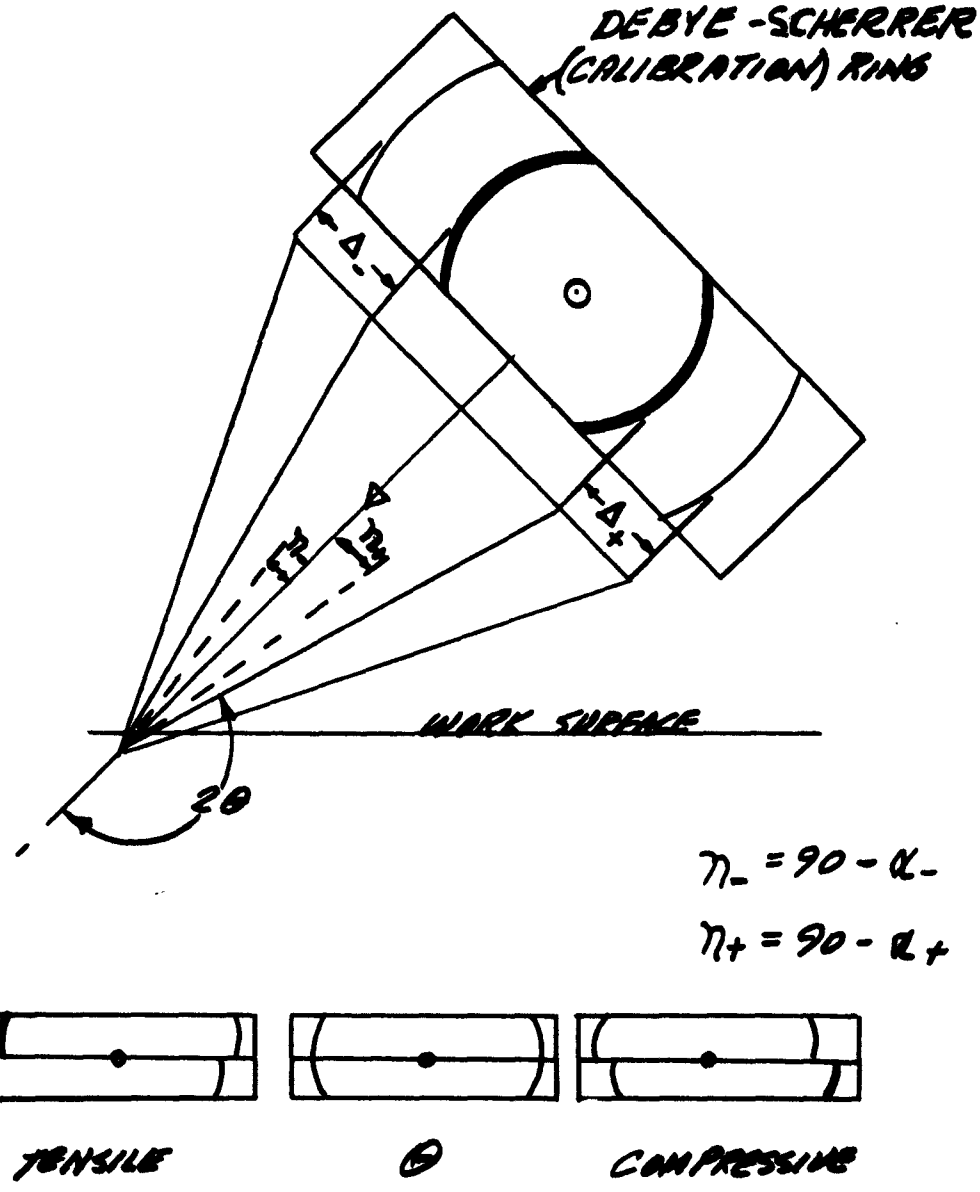

Figure 9

NON-DESTRUCTIVE TESTING, INSPECTION - PYROLYTIC GRAPHITE

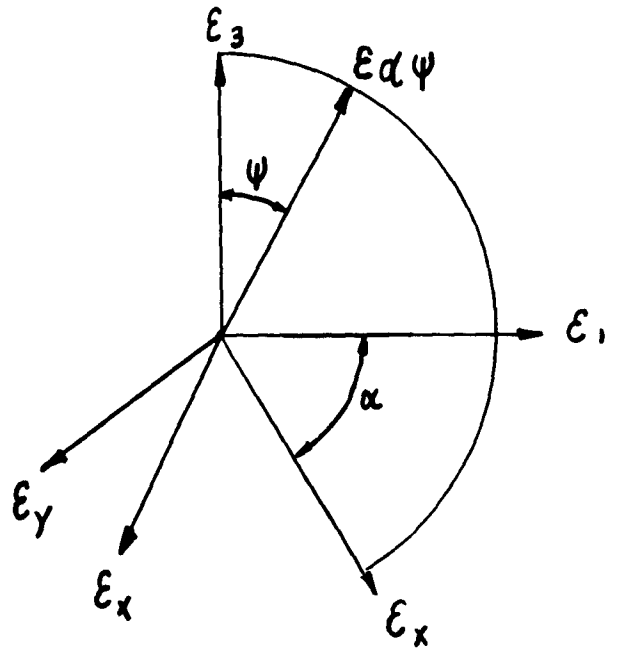

Figure 10A

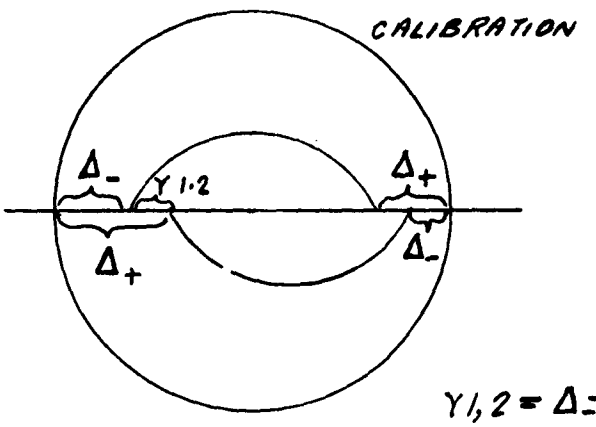

Figure 10B

$\gamma_{1,2} = \Delta_- - \Delta_+ > 0$ TENSION STRESS

$\gamma_{1,2} = \Delta_- - \Delta_+ < 0$ COMPRESSION STRESS

Figure 10

5.3.7 Thermal Gradient Method - In principal, the infrared non-destructive testing technique is simple. The structure to be tested is heated or cooled in some convenient though controlled manner; while heating or cooling is going on, the surface of the test specimen is scanned with an infra-red radiation detector. Small differences in the intensity of the radiation at the surface are used to indicate the existence of flaws in the interior of the structure. Other variables, as emissivity factors, are taken into necessary calculations.

5.4 Performance Information and Data

This report section incorporates discussion results from specimens examined to illustrate each of the methods previously described. The sequence is similar to that of the previous section and follow in the below order.

1. Fluorescent Penetrant (5.4.1)
2. Ultrasonic (5.4.2)
3. Radiography (5.4.3)
4. Eddy-current (5.4.4)
5. X-ray Stress Analyzer (5.4.5)
6. Thermal Gradient (5.4.6)
7. Miscellaneous (5.4.7)

5.4.1 Examples of the penetrant tests are found in Figures 11, 12, 13 and 14. In the first case evidence of a crack is noted toward the upper edge of the specimen. The penetrant shows as an irregular white line. White specks in this photo indicate infirm nodules (See Figure 13), loosened at their periphery.

Additional cracks in this specimen are noted in Figure 14 also along the upper edge and one significant flaw in the center of the forward section.

Further illustrations of external flaw detection, or relative absence, are found in the subsequent photograph. (See Figure 15.)

Full size shapes were subjected to penetrant tests as well as ordinary specimens such as hemispheres, cylinders and some plate specimens.

These models were tested using Zyglo penetrant materials in accordance with Specification MIL I-6866, Type I fluorescent penetrant. Flaked areas retained some penetrant, as did cracks, sooty areas and miscellaneous surface inclusions.

NON-DESTRUCTIVE TESTING, INSPECTION - PYROLYTIC GRAPHITE

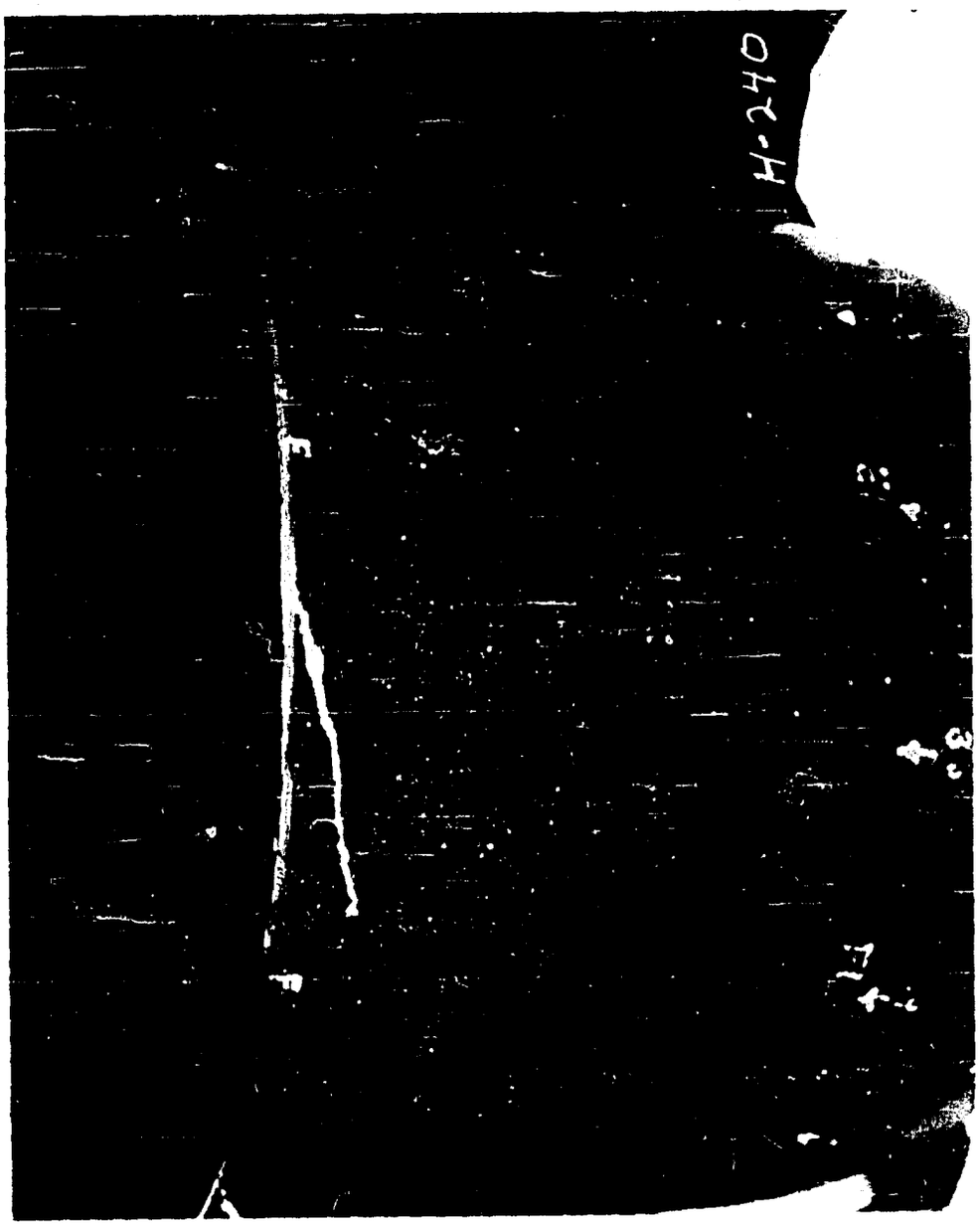

Figure 11

Penetrant Test - Edge and Nodule Defects.

NON-DESTRUCTIVE TESTING, INSPECTION - PYROLYTIC GRAPHITE

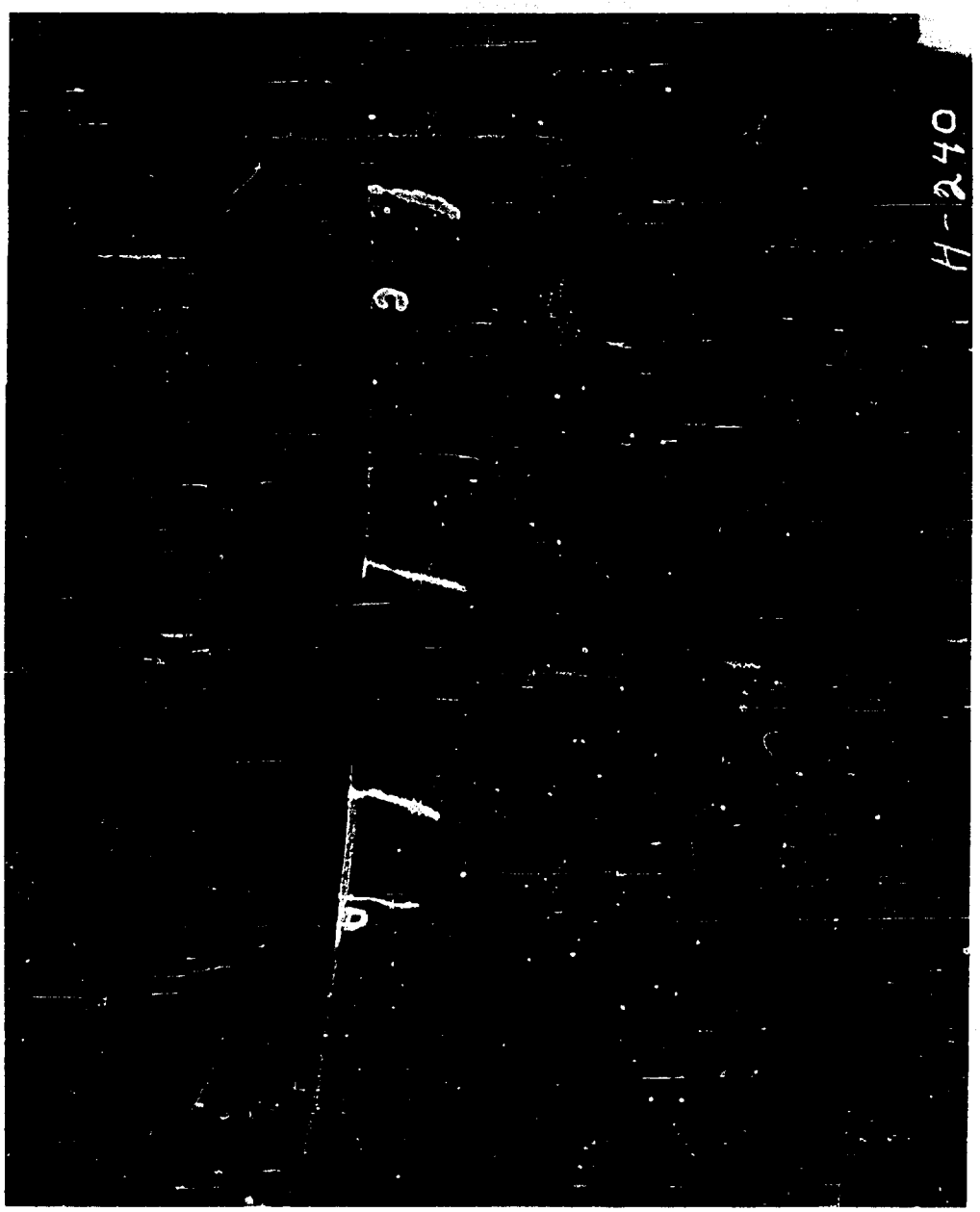

Figure 12

Penetrant Test - Edge and Nodule Defects.

NON-DESTRUCTIVE TESTING, INSPECTION - PYROLYTIC GRAPHITE

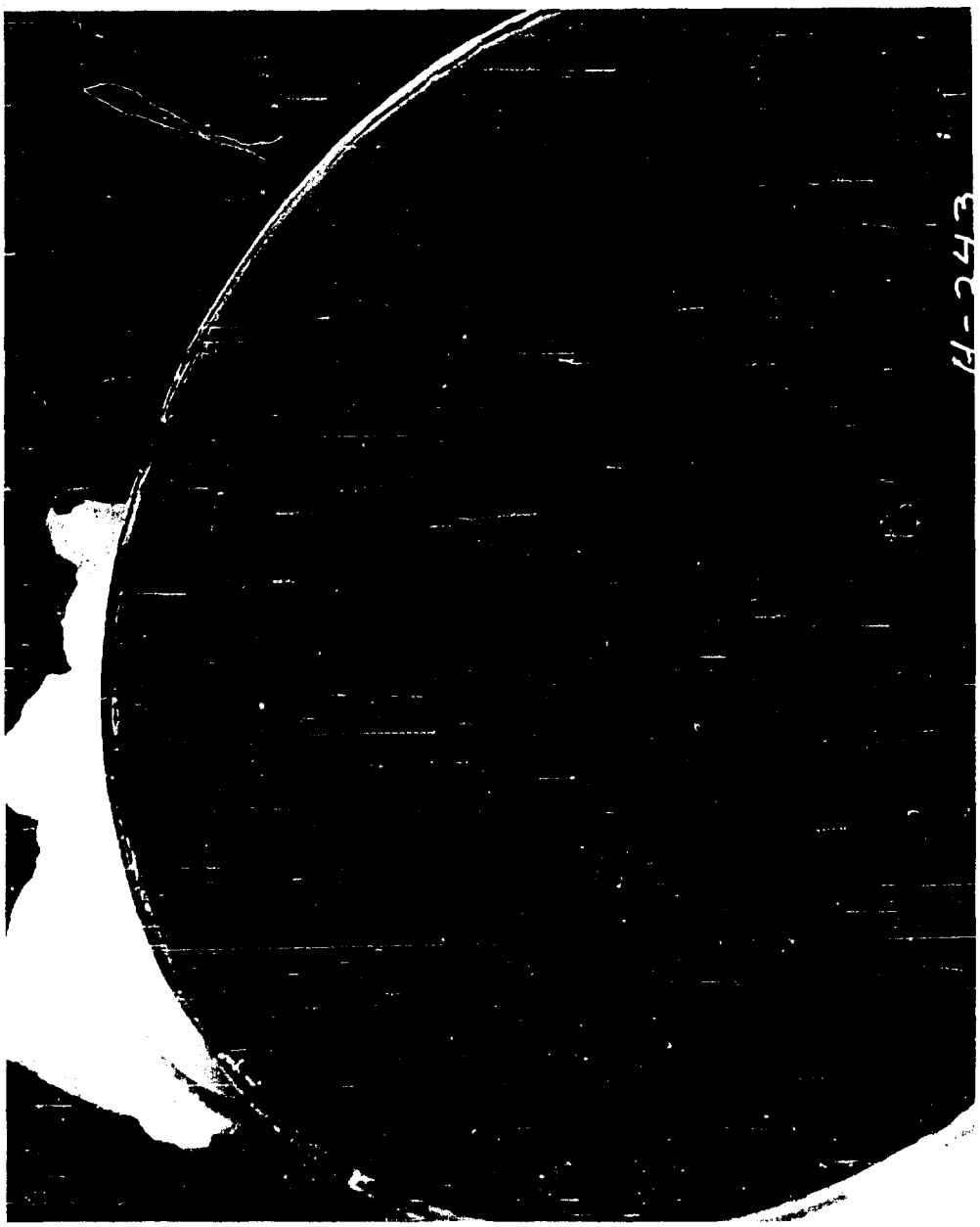

Figure 13

Penetrant Liquid Film on Inside Surface of a Cylinder.

NON-DESTRUCTIVE TESTING, INSPECTION - PYROLYTIC GRAPHITE

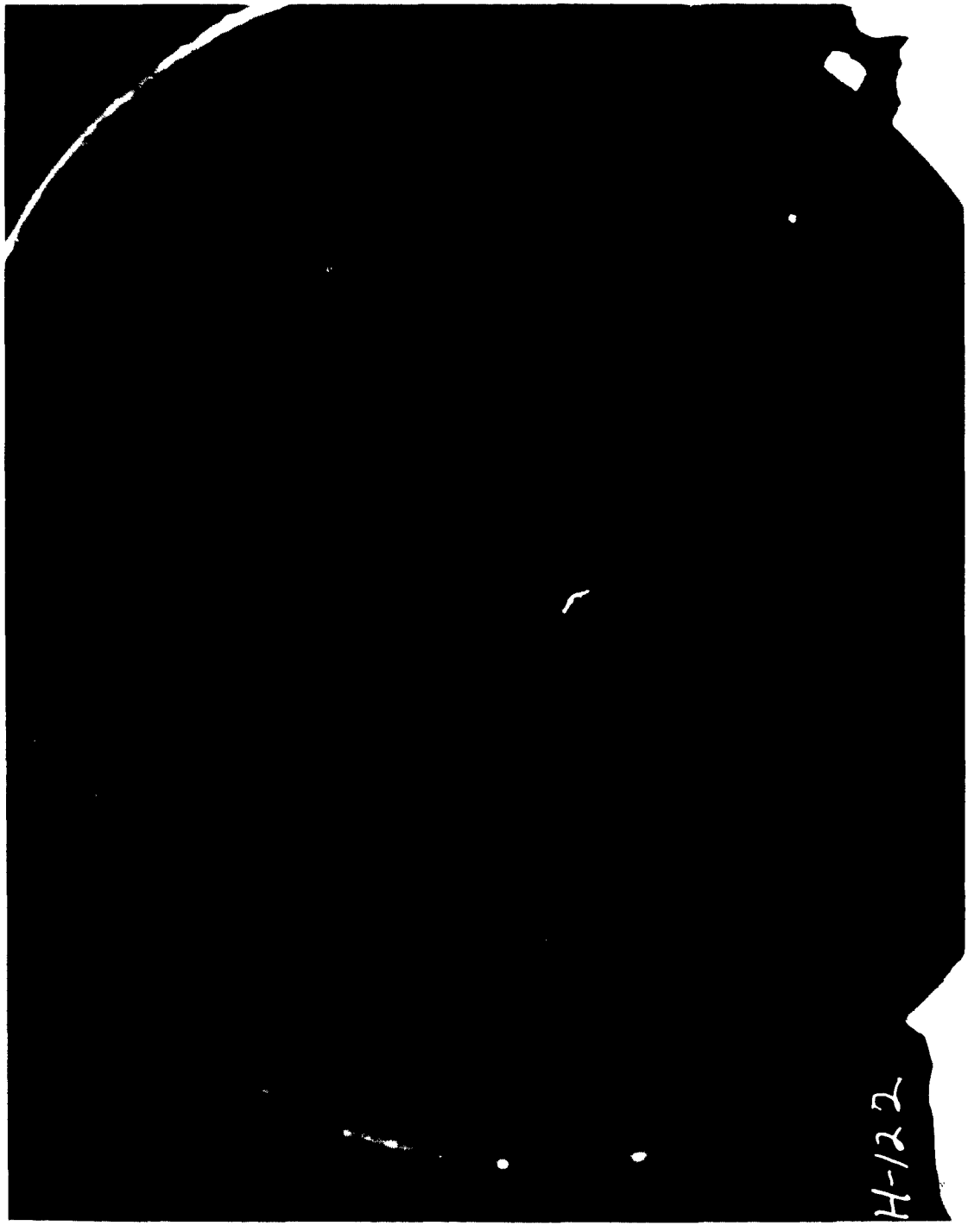

Figure 14

Penetrant Test - Large Nodule (Center) Defect and Lamination.

NON-DESTRUCTIVE TESTING, INSPECTION - PYROLYTIC GRAPHITE

Figure 15

Same Picture as Figure 14 Before Penetrant. Note Nodule and Lamination.

5.4.1.1 Somewhat in this same (penetrants) category it was desired to learn the effect, if any, of various chemical solutions. These were chosen from a list of materials with which graphite specimens were likely to come in contact during inspection, N-D testing and handling. The results of this investigation are found in Table 1.

5.4.2 Ultrasonic means of testing gave indicative information on the internal structure of all specimens examined by these methods. The Immerscope afforded recorded data that could be analyzed in comparison with results from other test methods. However, large models could not be accommodated by the immersion tank and for this reason a hand probe method was tried but considered too time consuming for practical purposes. Further, the hand probe did not produce a recorded trace which was most necessary for data processing.

Illustrative traces are found in Figure 16, A and B. The "A" trace is taken from a sound specimen with few minute and well distributed points of possible lamination. In "B", however, evidence of two distinct varieties of laminations are disclosed. The large "blot" in the lower center is an excellent recording of laminated area. In this instance, laminations occur as continuous, cone to cone, breaks in a parallel manner.

In the upper portion of "B", laminations of a different nature are shown. In this area these imperfections occur first in one cone, on a given plane, and then another on, however, a different plane. The interrupted trace lines illustrate this feature in a manner to suggest large nodules are responsible to some extent. (See Appendix A, Figure 2, A and B.)

In Figure 17, a typical drill and ream operational specimen is shown. The effect of this work is depicted by the ultrasonic trace (Figure 18). It is seen in this trace that some, though slight, delaminations occur around the drilled and reamed areas.

Similar traces of an ultrasonically machined specimen is found in Figure 19B.

5.4.3 The use of radiography, or X-ray, analysis was extensively employed by Organization 71-22 (N.D.T.) throughout the program. Most all of the flat plates and small shapes were radiographed. All large models received were inspected by this method. As an aid in locating and defining imperfections a coded pattern was designed for classification of these defects. This classification is shown in Figure 20.

NON-DESTRUCTIVE TESTING, INSPECTION - PYROLYTIC GRAPHITE

Table IV - Immersion Tests - Pyrolytic Graphite

Solution	Weight Sample Number	Weight Before Immersion Grams	Thickness Before Immersion Inches	Weight After Immersion Grams	Thickness After Immersion Inches	Weight Difference Grams	Thickness Difference Inches
#1 Photo-Flo	1	3.6845	0.1082	3.6841	0.1080	-0.0004	-0.0002
	2	3.6032	0.1024	3.6028	0.1021	-0.0008	-0.0003
#2 KS-100	1	3.5896	0.1028	3.5908	0.1030	+0.0012	+0.0002
	2	3.5852	0.1028	3.5861	0.1028	+0.0009	0.0000
#3 P-145	1	3.7985	0.1042	3.7121	0.1038	-0.0864	-0.0004
	2	3.7382	0.1073	3.7374	0.1067	+0.0002	-0.0006
#4 P-146	1	3.7271	0.1077	3.7273	0.1076	+0.0002	-0.0001
	2	3.7887	0.1076	3.7901	0.1074	+0.0014	-0.0002
#5 ZZ-2	1	3.5579	0.1017	3.5569	0.1014	-0.0010	-0.0003
	2	3.7443	0.1080	3.7494	0.1081	+0.0051	+0.0001
#6 ZB-2	1	3.7516	0.1059	3.7506	0.1055	-0.0010	-0.0004
	2	3.7341	0.1062	3.7348	0.1056	+0.0007	-0.0006
#7 ZZ-5	1	3.6396	0.1037	3.6401	0.1036	+0.0005	-0.0001
	2	3.5742	0.1030	3.5734	0.1030	-0.0008	0.0000
#8 M.E.K.	1	3.6159	0.1073	3.6164	0.1073	+0.0005	0.0000
	2	3.6353	0.1015	3.6351	0.1010	-0.0002	-0.0005
#9 MB-37-1009	1	3.6682	0.1089	3.6699	0.1047	+0.0007	+0.0018
	2	3.6692	0.1068	3.6682	0.1063	-0.0010	-0.0005
#10 Carbon Tetrachloride	1	3.6115	0.1018	3.6124	0.1018	+0.0009	0.0000
	2	3.5697	0.1016	3.5702	0.1010	+0.0005	-0.0006
#11 #2 Spotcheck	1	3.4476	0.1058	3.4484	0.1056	+0.0008	-0.0002
	2	3.7553	0.0998	3.7583	0.0995	+0.0030	-0.0003
#12 #3 Spotcheck	1	3.6976	0.1037	3.7004	0.1045	+0.0028	+0.0008
	2	3.6642	0.1031	3.6653	0.1030	+0.0011	-0.0001

NON-DESTRUCTIVE TESTING, INSPECTION - PYROLYTIC GRAPHITE

Table I - Continued

Solution	Sample Number	Weight Before Immersion Grams	Thickness Before Immersion Inches	Weight After Immersion Grams	Thickness After Immersion Inches	Weight Difference Grams	Thickness Difference Inches
#13 ZS-7	1	3.7060	0.1028	3.7506	0.1028	+0.0446	0.0000
	2	3.4235	0.1064	3.4346	0.1071	+0.0111	+0.0007
#14 ZL-22	1	3.7841	0.1072	3.7871	0.1021	+0.0030	-0.0001
	2	3.5668	0.1037	3.5707	0.1024	+0.0039	-0.0013
#15 ZP-7	1	3.7542	0.1058	3.7555	0.1057	+0.0013	-0.0001
	2	3.5132	0.0996	3.5145	0.0996	+0.0013	0.0000
#5 & #6 ZL2 & ZL-2	1	3.5569	0.1014	3.5585	0.1016	+0.0016	+0.0002
	2	3.7494	0.1081	3.7486	0.1078	-0.0008	-0.0003
#7 & #8 H.E.C. & ZP-5	1	3.6164	0.1073	3.6173	0.1072	+0.0009	-0.0001
	2	3.6351	0.1010	3.6359	0.1013	+0.0008	+0.0003
#11 & #12 Spectasol #2 & Spectasol #3	1	3.4484	0.1056	3.4496	0.1055	+0.0012	-0.0001
	2	3.7583	0.0995	3.7576	0.0995	-0.0007	0.0000
#13 & #14 ZS-7 & ZL-22	1	3.7506	0.1028	3.7073	0.1030	-0.0433	+0.0002
	2	3.4346	0.1701	3.4251	0.1066	-0.0095	-0.0005
#13, #14 & #15 ZS-7, ZL-22, ZP-7	1	3.7073	0.1030	3.7038	0.1029	-0.0035	-0.0001
	2	3.4251	0.1066	3.4231	0.1066	-0.0020	0.0000

NON-DESTRUCTIVE TESTING, INSPECTION - PYROLYTIC GRAPHITE

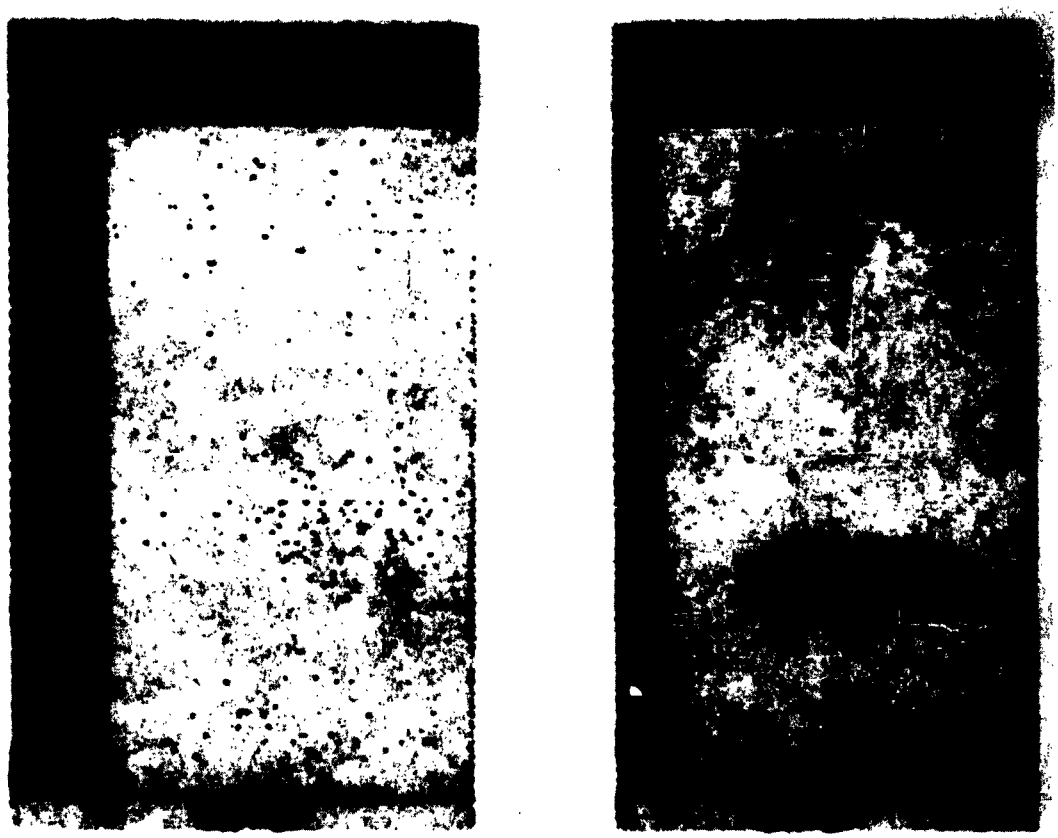

A B

Figure 16

Ultrasonic Traces

NON-DESTRUCTIVE TESTING, INSPECTION - PYROLYTIC GRAPHITE

DEPOSITION SURFACE

MANDREL SURFACE

MACHINING METHOD: DRILL, DRILL & REAM,
END MILL
FROM DEPOSITION SURFACE

NO SUPPORT

Figure 17

NON-DESTRUCTIVE TESTING, INSPECTION - PYROLYTIC GRAPHITE

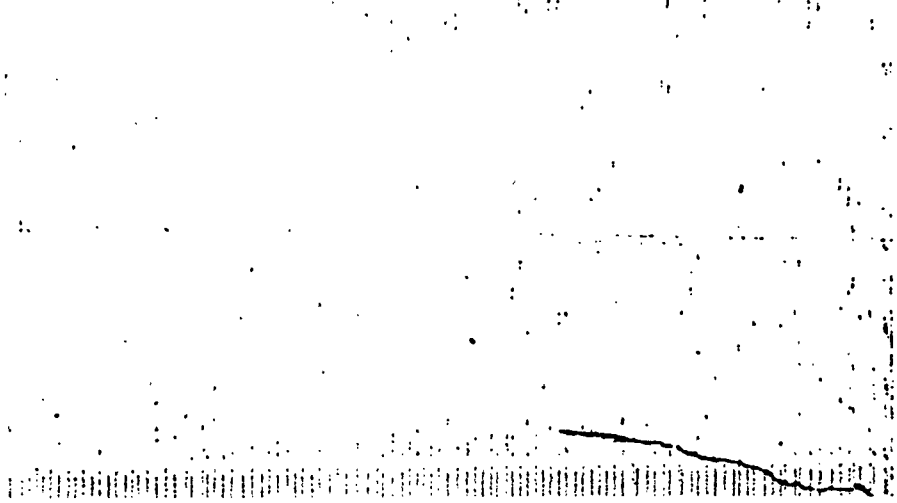

BEFORE MACHINING

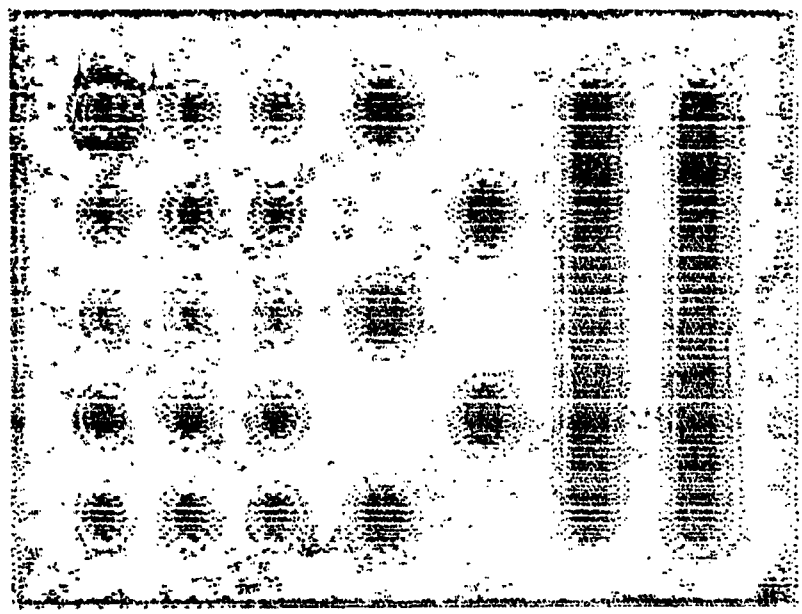

AFTER MACHINING
ULTRASONIC TRACES OF DRILL, REAMED
& MILLED SPECIMEN

Figure 18

NON-DESTRUCTIVE TESTING, INSPECTION - PYROLYTIC GRAPHITE

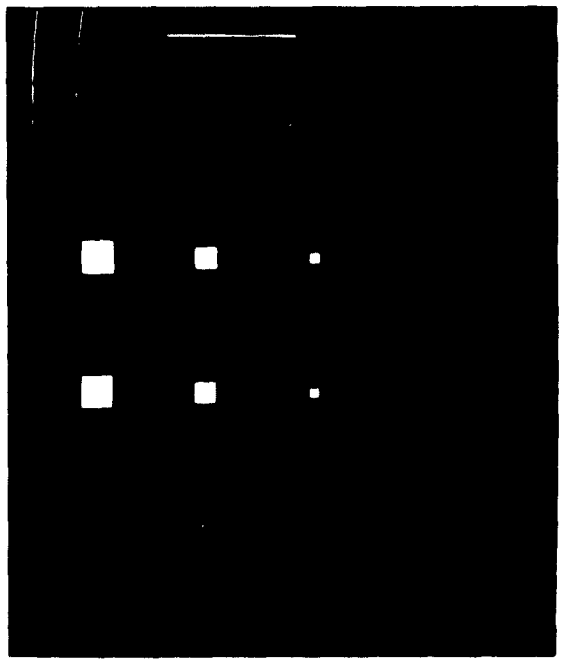

Figure 19A

Ultrasonic Inspection Test Blocks Blind Holes and Slots Machined by Ultrasonic Methods - Edges and Surfaces Conventionally Ground.

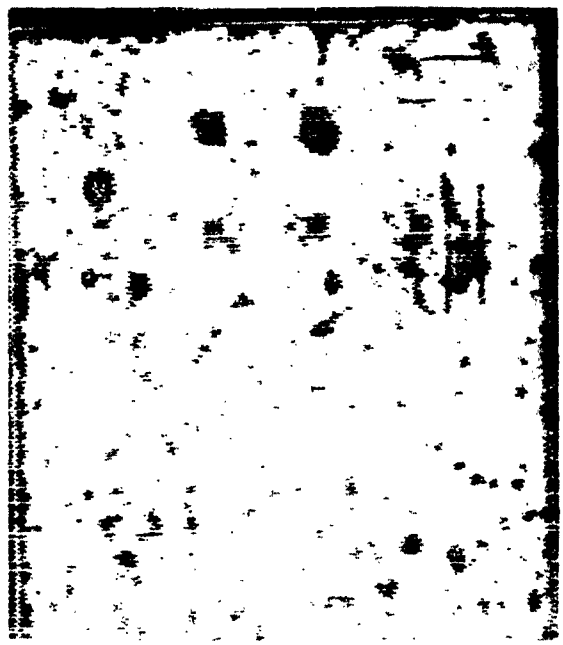

Figure 19B

Trace Results from Work on Test Blocks.

Figure 19

Trace Results from Ultrasonic Machine Work on Test Blocks

NON-DESTRUCTIVE TESTING, INSPECTION - PYROLYTIC GRAPHITE

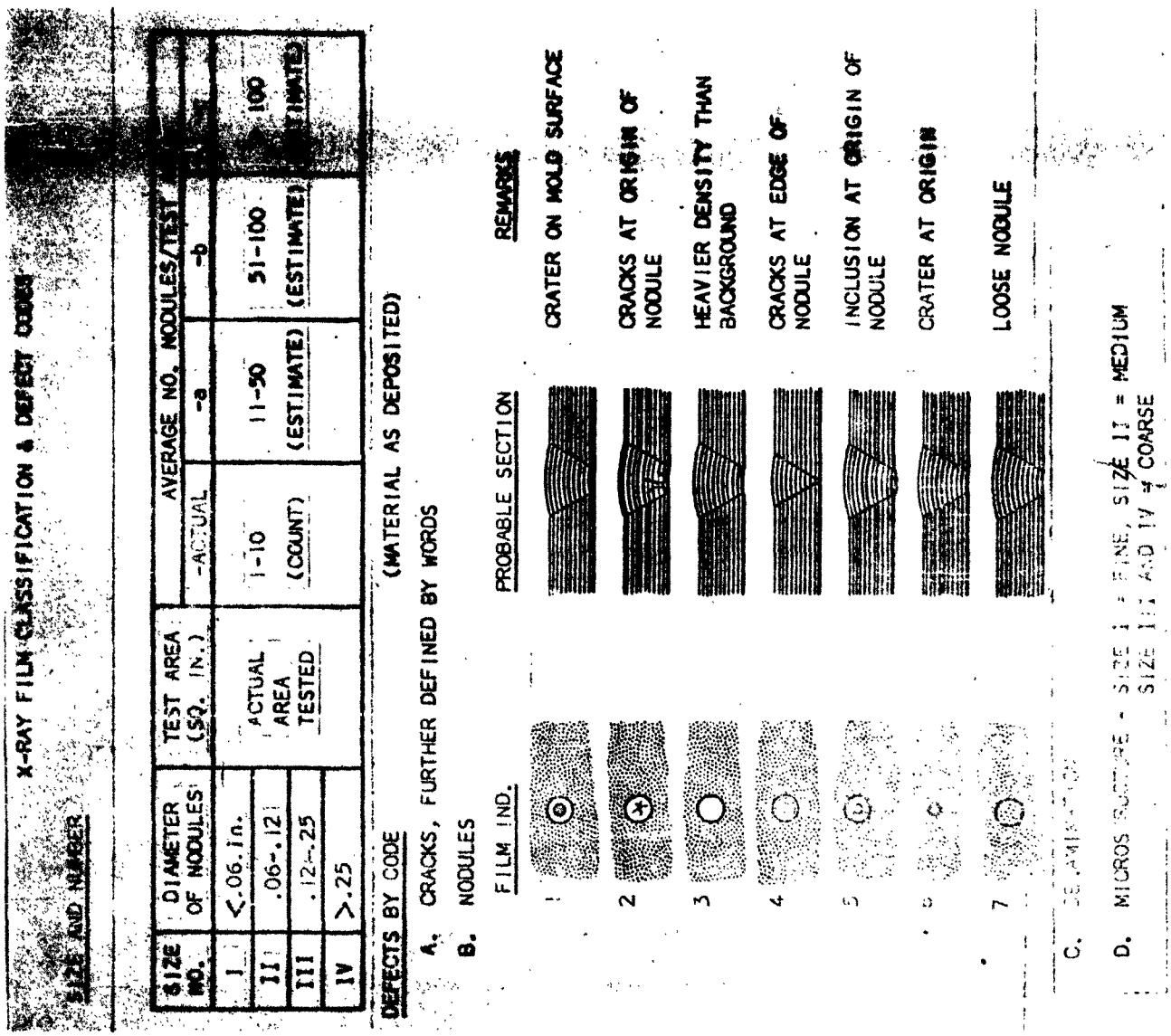

Figure 20

X-Ray Film Classification and Defect Codes

NON-DESTRUCTIVE TESTING, INSPECTION - PYROLYTIC GRAPHITE

In the early stages of the program frequently larger specimens contained all seven defects as illustrated. This situation, however, became considerably relieved as supplier's production methods were improved. The uniformity and quality of materials were so improved towards latter stages of the program that seldom more than three of the defect types were noticeable.

One illustration of a typed defect is found in the X-ray photographs in Figure 21 and 22. In approximately the center of Figure 21 a defect (type 5) is plainly visible; Figure 22 shows this same defect but examined from an oblique angle thus revealing the interrupted spiral layers of the nodule. This particular X-ray was made on a large scale shape which had been machined. The circular tool marks are faintly discernible.

Other examples of pattern type defects are found in Figure 23 and 24.

All radiographs were made in accordance with M-I-6865, Amendment 2; different angles, exposure times and voltages were tried to assure accomplishment of lightest possible details.

5.4.4 Eddy-Current - This method was established as being unique in sensing one significant characteristic of pyrolytic graphite. For example, it is well known that this material radiates heat exceptionally well in the "a" direction but conducts heat only slightly in the "c" direction. By analysis of this phenomena, it is clear that the more uniform the layer planes the more efficiently heat is both radiated in one direction and blocked in the other; thus paralellism of layer planes is an important property to consider when testing pyrolytic graphite.

By use of Eddy-Current (Radac Model 302 - The Budd Company) it was possible to closely estimate the degree of parallelism in specimens under test. This can only be accomplished with the Lockheed facility available through Organization 71-22. This apparatus is equipped with both a primary circuit and a secondary or memory circuit which allows conductivity reading by differential methods.

A test was conducted on especially prepared specimens wherein each was angularly machined through layer planes. This simulated lack of parallelism in specific degree increments, viz., $1/2^{\circ}$, 1°, $1\text{-}1/2^{\circ}$ and 2° respectively in four samples. Under eddy-current observation, conductivity in the "c" direction became progressively more pronounced as the angular cut increased. These samples had been previously indexed on a Rotab instrument and the conductivity results are significant in confirmation of simulated lack of parallelism.

NON-DESTRUCTIVE TESTING, INSPECTION - PYROLYTIC GRAPHITE

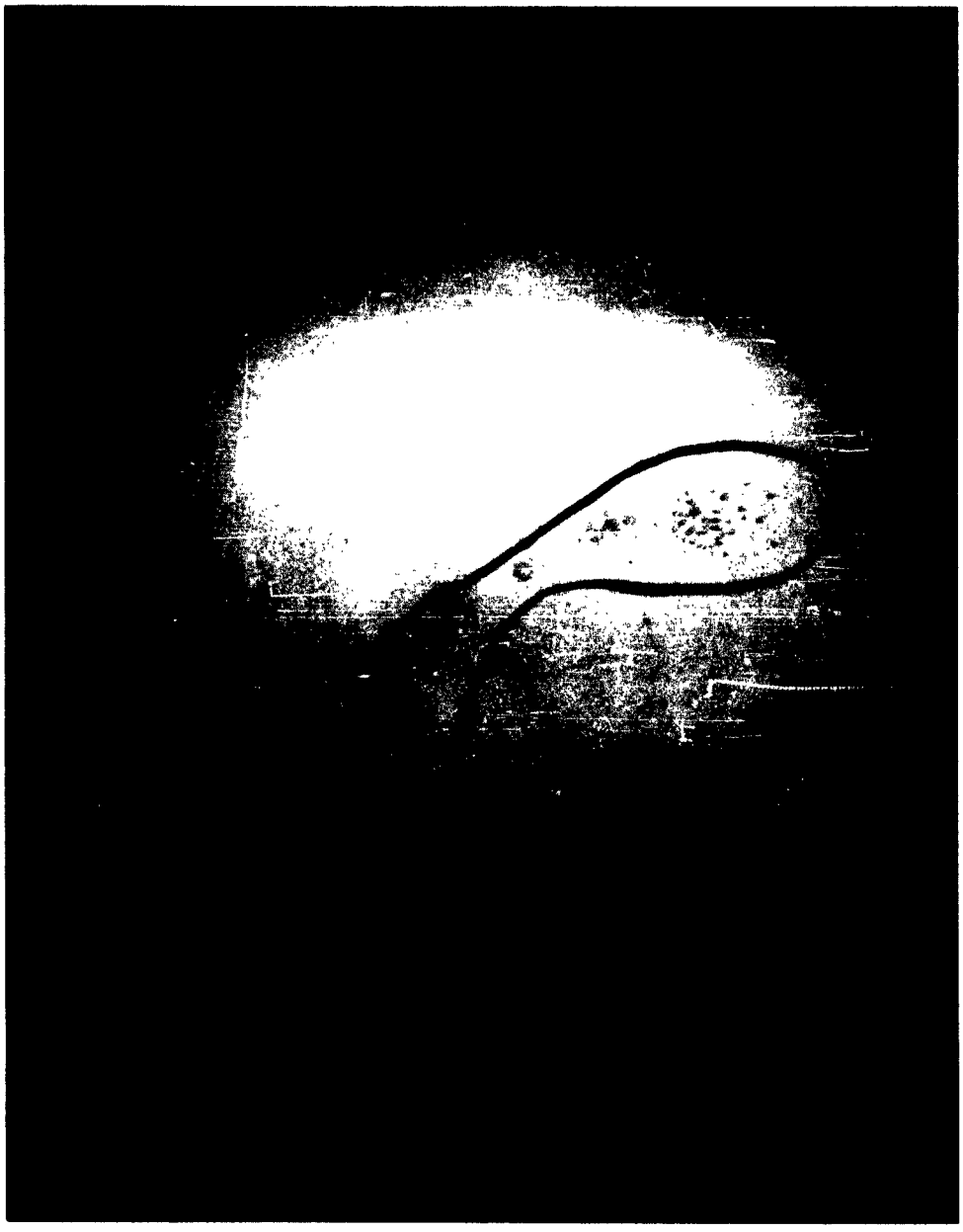

Figure 21

Family of Defects Disclosed by X-Ray Examination (Marked Area).

NON-DESTRUCTIVE TESTING, INSPECTION - PYROLYTIC GRAPHITE

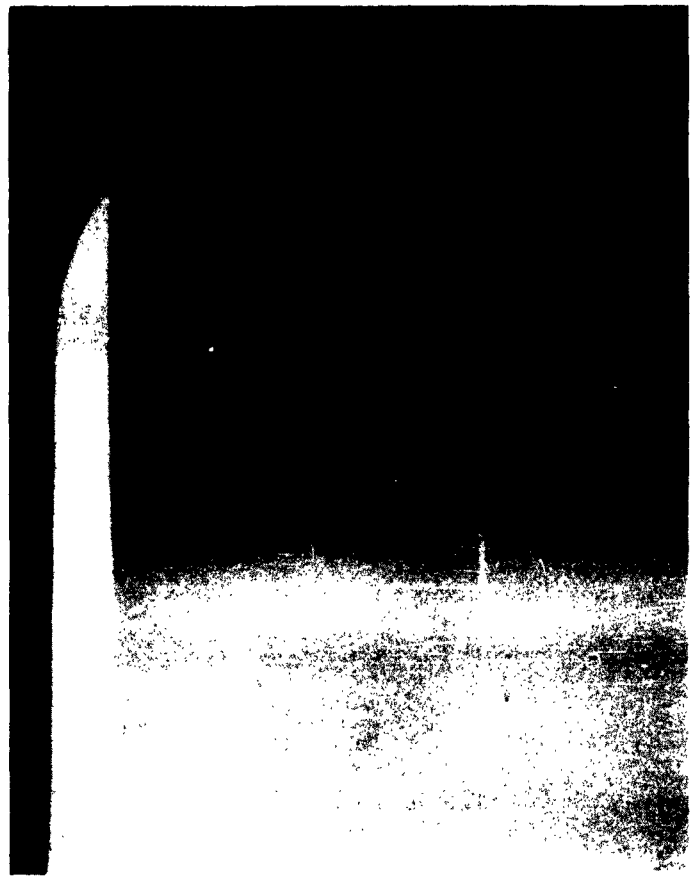

Figure 22

Nodule Defect (Center Figure 21) Filmed from Oblique Angle.

NON-DESTRUCTIVE TESTING, INSPECTION - PYROLYTIC GRAPHITE

Figure 23

Cracks at Edge of Large Nodules.

NON-DESTRUCTIVE TESTING, INSPECTION - PYROLYTIC GRAPHITE

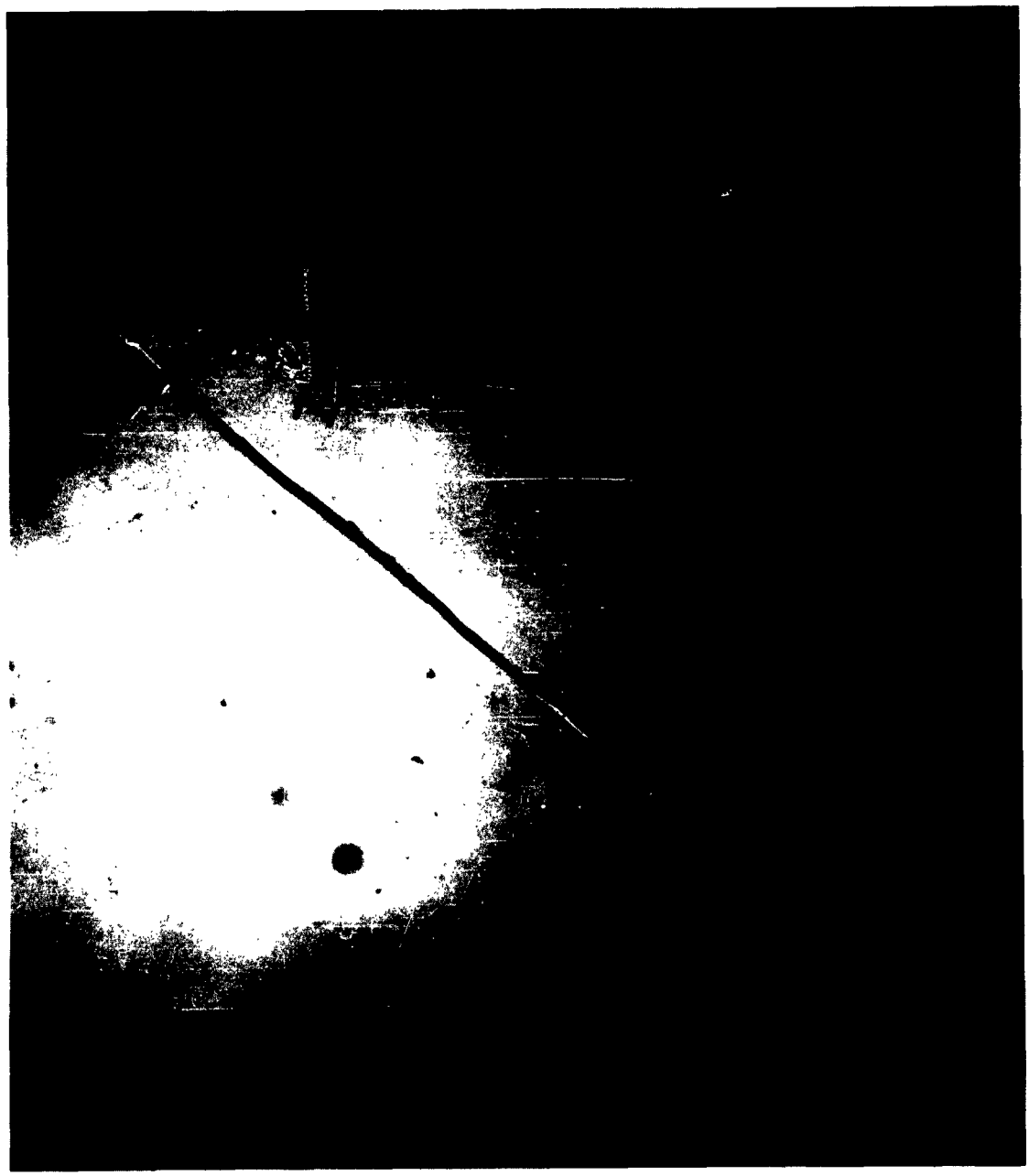

Figure 24

Loose Nodules by X-Ray Examination.

NON-DESTRUCTIVE TESTING, INSPECTION - PYROLYTIC GRAPHITE

It is expected that a set of standards, based upon "c" conductivity, can be established upon resumption of the feasibility program.

5.4.5 X-Ray Stress Analyzer - Residual stress measurements on pyrolytic graphite, by X-ray stress analyzer methods, did not prove as simple as when the same method is used on metals. However, no insurmountable problems were encountered and the information gathered is of considerable significance.

Examination of plates and shapes disclosed areas of high residual stress in both tension and compression in relatively short distances. Measurements on some specimens were occasionally as high as 7500 psi; a more normal figure of 1500-2000 was frequently evident.

The illustration in Figure 25 shows an example of the Debye-Scherrer ring as found in pyrolytic graphite analyses and the mis-alignment described earlier in this report. (Procedures, Paragraph 5.3.5.) This figure illustrates the difficulty of accurate measurements of mis-alignment without the aid of a light densitometer.

Figure 26 discloses the distinctiveness of the Debye-Scherrer ring in metals.

Since visual measurement is impractical, the extent of mis-alignments found in test specimens were determined by the light densitometer. This instrument is illustrated in Figure 27 and 28. An approximation of typical findings are shown by dotted lines on the photographs in Figure 29. The mis-alignment therefore becomes measureable and the difference in millimeters is the basis for stress calculations converted to pounds per square inch. The accuracy of these methods of both test and calculation was well demonstrated by proven reproducibility and repeatability periodically undertaken.

An illustration of the internal stresses, both tension and compression, are found in the accompanying Chart 1. This particular specimen was drilled in increments of 0.030" depth. An X-ray stress analysis was made at each depth with results as shown in the chart. The calculated pounds per square inch stresses are shown in Table 2.

NON-DESTRUCTIVE TESTING, INSPECTION - PYROLYTIC GRAPHITE

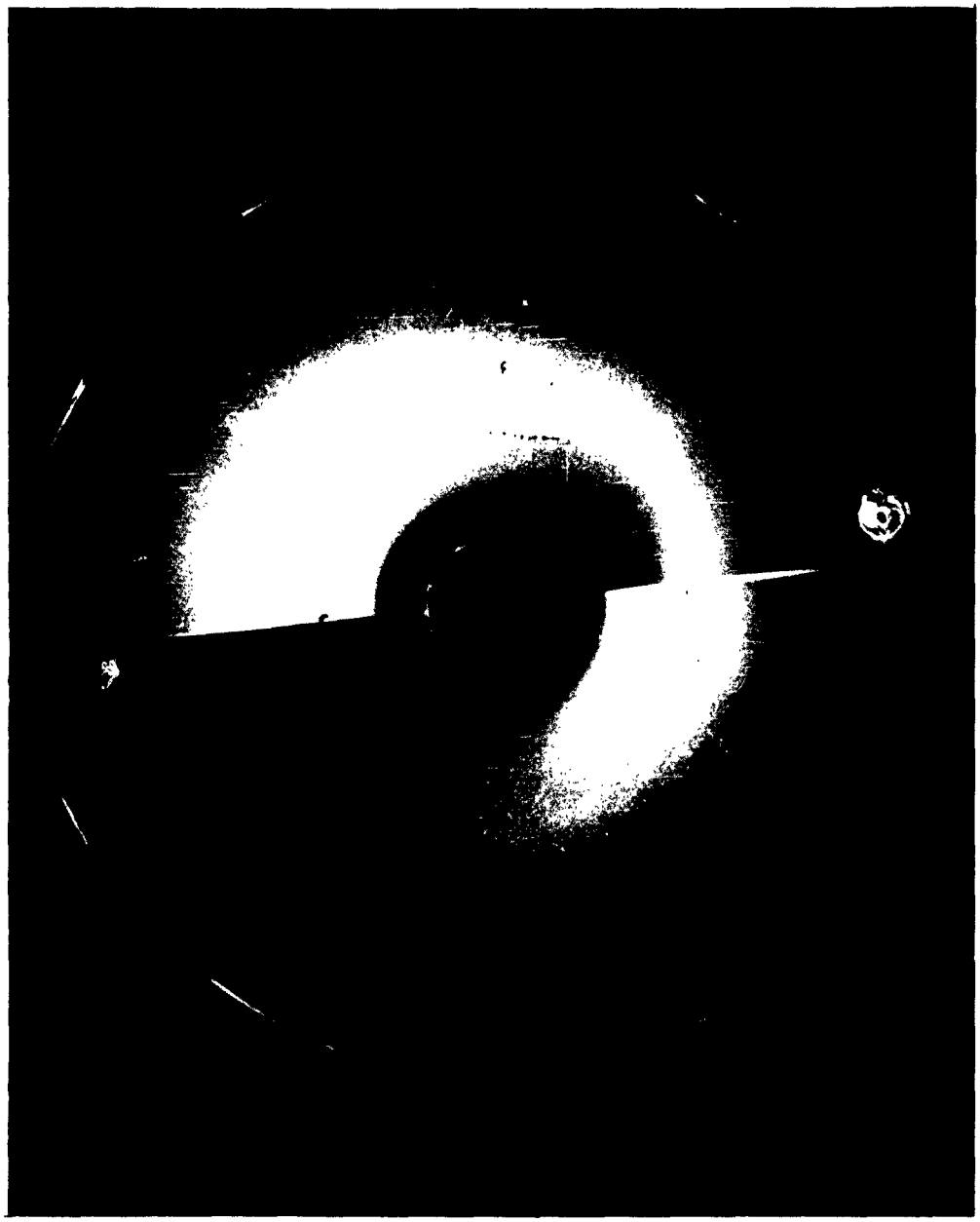

Figure 25

Debye-Scherrer Ring in Pyrolytic Graphite.

NON-DESTRUCTIVE TESTING, INSPECTION - PYROLYTIC GRAPHITE

Figure 25

Debye-Scherrer Ring in Pyrolytic Graphite.

NON-DESTRUCTIVE TESTING, INSPECTION - PYROLYTIC GRAPHITE

Figure 26

Debye-Scherrer Ring in Magnesium.

NON-DESTRUCTIVE TESTING, INSPECTION - PYROLYTIC GRAPHITE

Figure 27

Light Densitometer.

NON-DESTRUCTIVE TESTING, INSPECTION - PYROLYTIC GRAPHITE

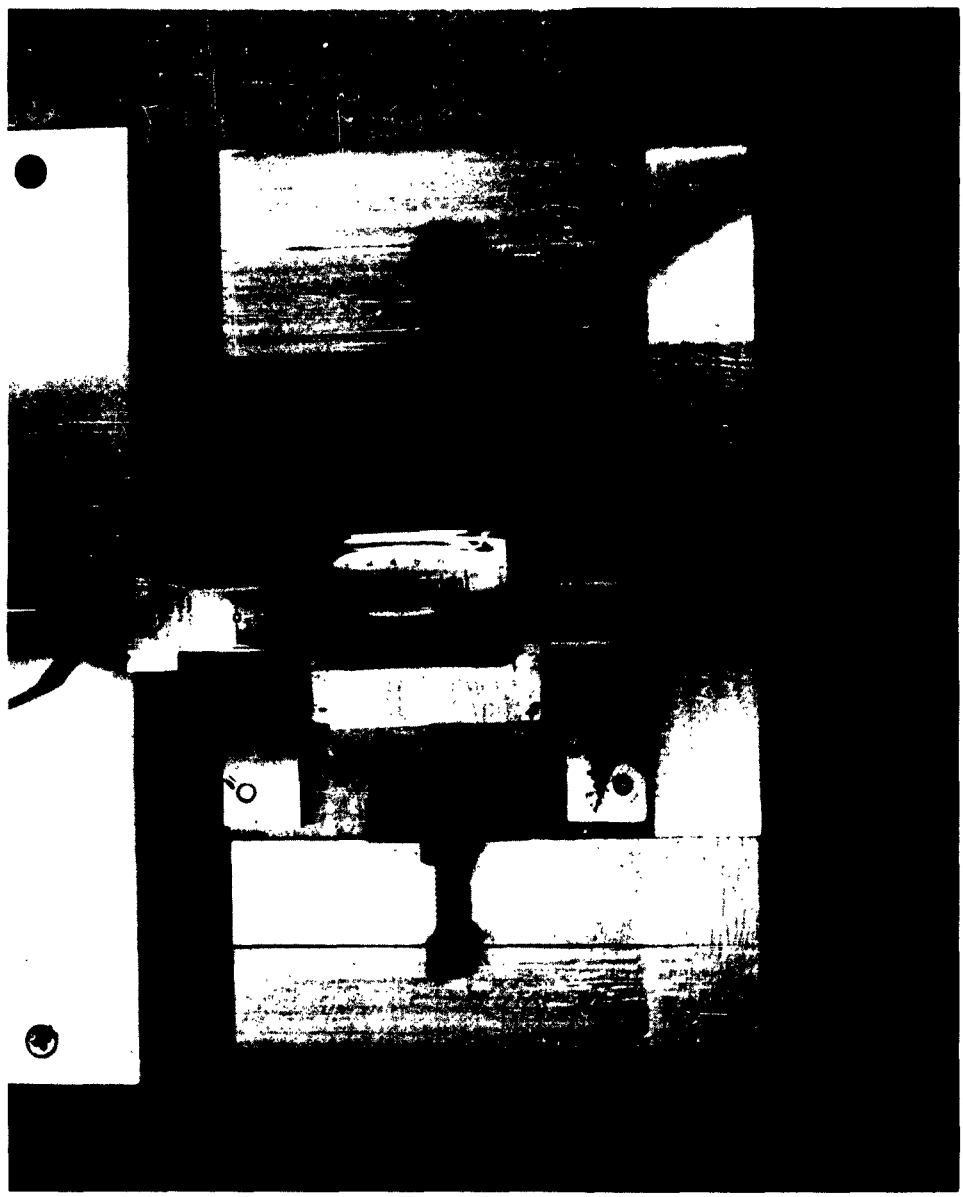

Figure 28
Densitometer Vernier for Measurement
of Misalignment in Debye-Scherrer Ring.

NON-DESTRUCTIVE TESTING, INSPECTION - PYROLYTIC GRAPHITE

Figure 29
Dotted Line Illustrating Light Density
on Sample Shown in Figure 25.

NON-DESTRUCTIVE TESTING, INSPECTION - PYROLYTIC GRAPHITE

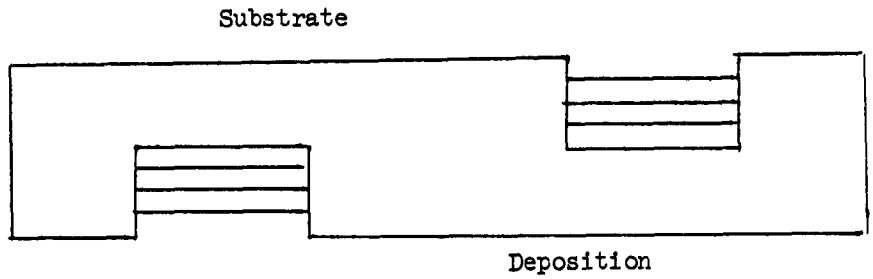

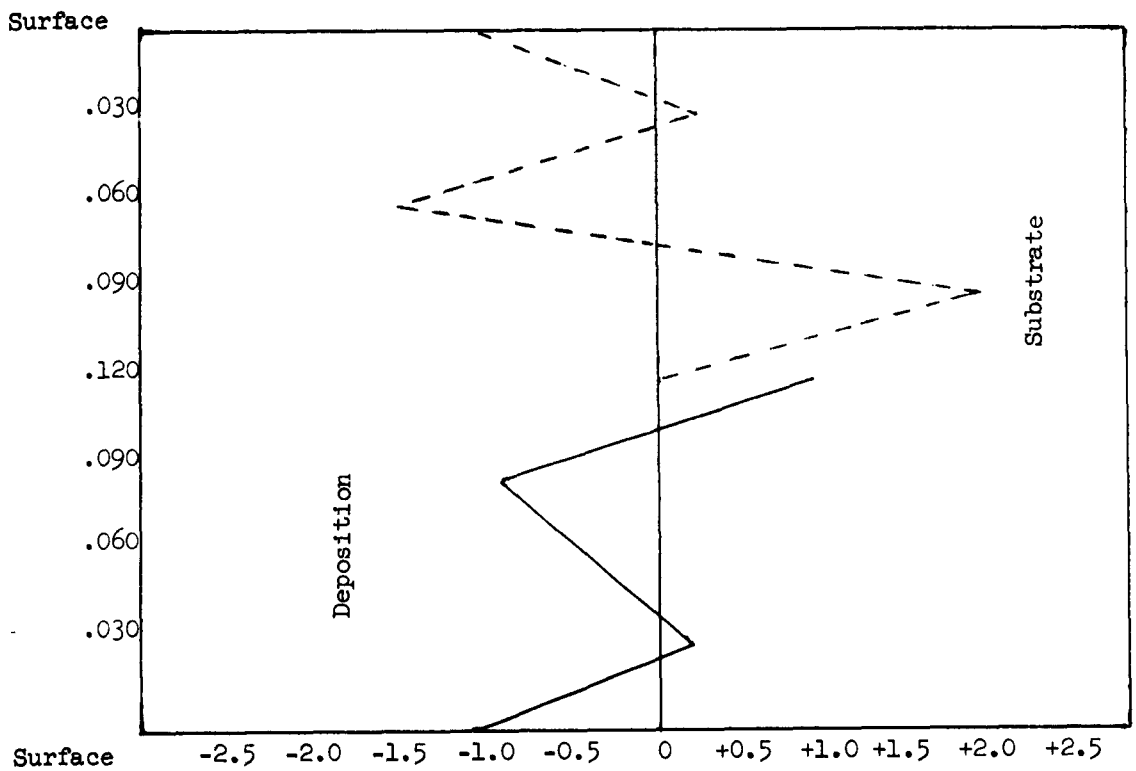

Millimeters Off-Set

Chart 1

Stress Analysis H-317

NON-DESTRUCTIVE TESTING, INSPECTION - PYROLYTIC GRAPHITE

Surface	+ MM Offset	- MM Offset	PSI Tension	Compression
Substrate		0.95		1909
Substrate	0.25		502	
Substrate		1.50		3016
Substrate	1.95		3920	
Deposition	0.95		1909	
Deposition		0.95		1909
Deposition		0.60		1206
Deposition	0.20		402	
Deposition		1.05		2111

Table 2

Stress Analysis
(From Chart 1)

NON-DESTRUCTIVE TESTING, INSPECTION - PYROLYTIC GRAPHITE

5.4.6 The feasibility of non-destructively testing pyrolytic graphite by thermal gradient methods was briefly evaluated. A development unit capable of study in this connection was located in Palo Alto in Communications and Controls, Organization 58-11.

Priority of work on another program precluded extensive tests by the department (58-11). However one evaluation series indicated promising aspects of the method. For instance, three flat samples were first radiographically and ultrasonically tested. These were then scanned with the thermal gradient apparatus. This experiment demonstrated that delaminations in pyrolytic graphite were extremely easy to detect. The specimens internal structure appears equally detailed with that revealed by ultrasonic methods.

A typical thermal gradient trace, Figure 30, of a pyrolytic graphite specimen follows. The extreme dips or valleys illustrate imperfections and were correlated as such by both X-ray and ultrasonic test methods.

An understanding of thermal gradient approach may be obtained from the following discussions and photographs. Figure 31 illustrates a partial view of the apparatus.

The graphite sample was heated to a temperature above room temperature by an amount too small to measure by the thermocouples used. Pronounced structure was observed upon scanning the sample with the gradient detector. In general, the structure was equally pronounced in the thermal gradient detector as in the ultrasonic record. In view of this fact, observable detail would increase rapidly with higher test temperature, and inasmuch as pyrolytic graphite can be heated to temperatures well in excess of the boiling point of water without damage, it appears to be certain that more structural detail can be resolved than exists in delamination (Figure 30) patterns alone (e.g. small variations in thickness and density).

This pyrolytic graphite program was discontinued before an opportunity was realized to fully exploit the capability of thermal gradient as a N-D method. It is recommended, however, that the method be further investigated should the program be resumed at any time in the future.

Accompanying photographs show the thermal gradient unit and accessories as developed by Organization 58-11. (Figures 32, 33, 34 and 35.)

NON-DESTRUCTIVE TESTING, INSPECTION - PYROLYTIC GRAPHITE

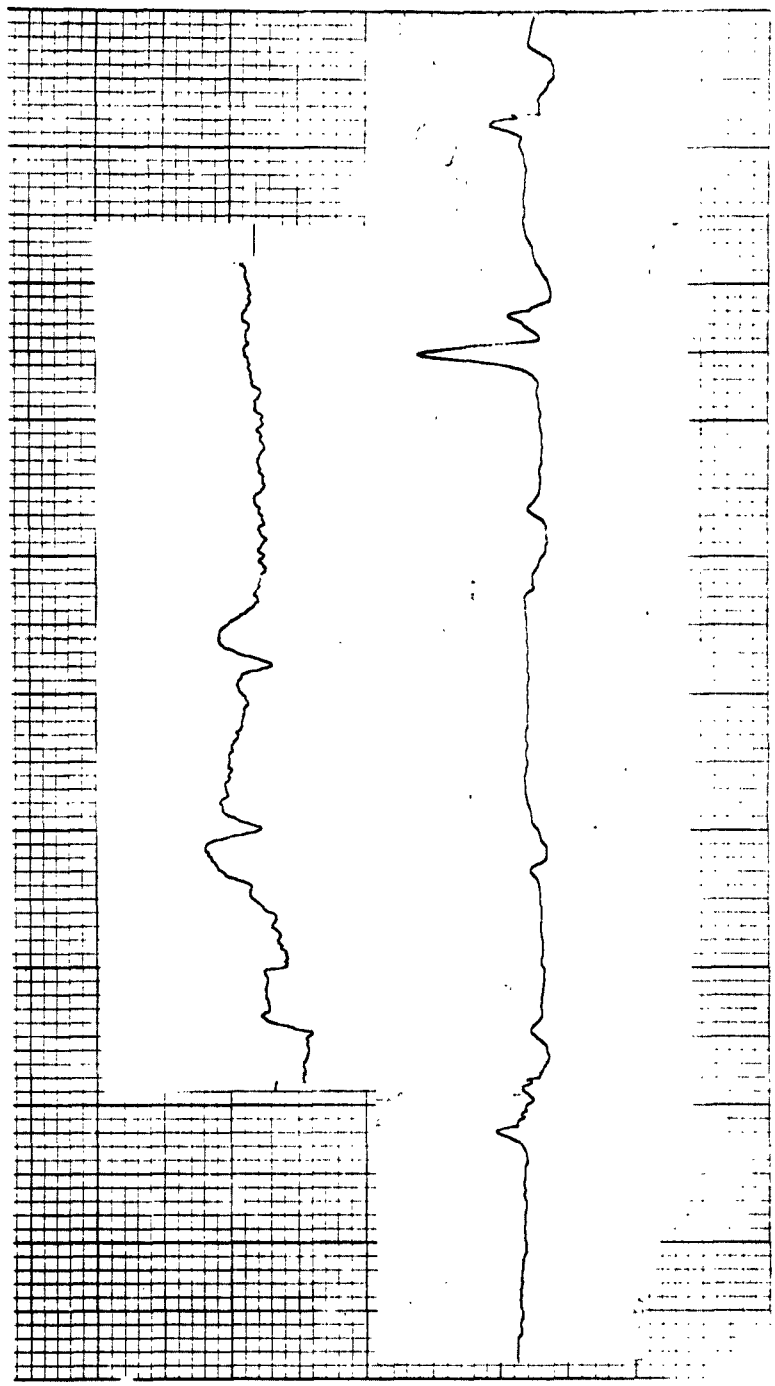

Figure 30

Thermal Gradient (Infra-red) Trace of Pyrolytic Graphite Samples

NON-DESTRUCTIVE TESTING, INSPECTION - PYROLYTIC GRAPHITE

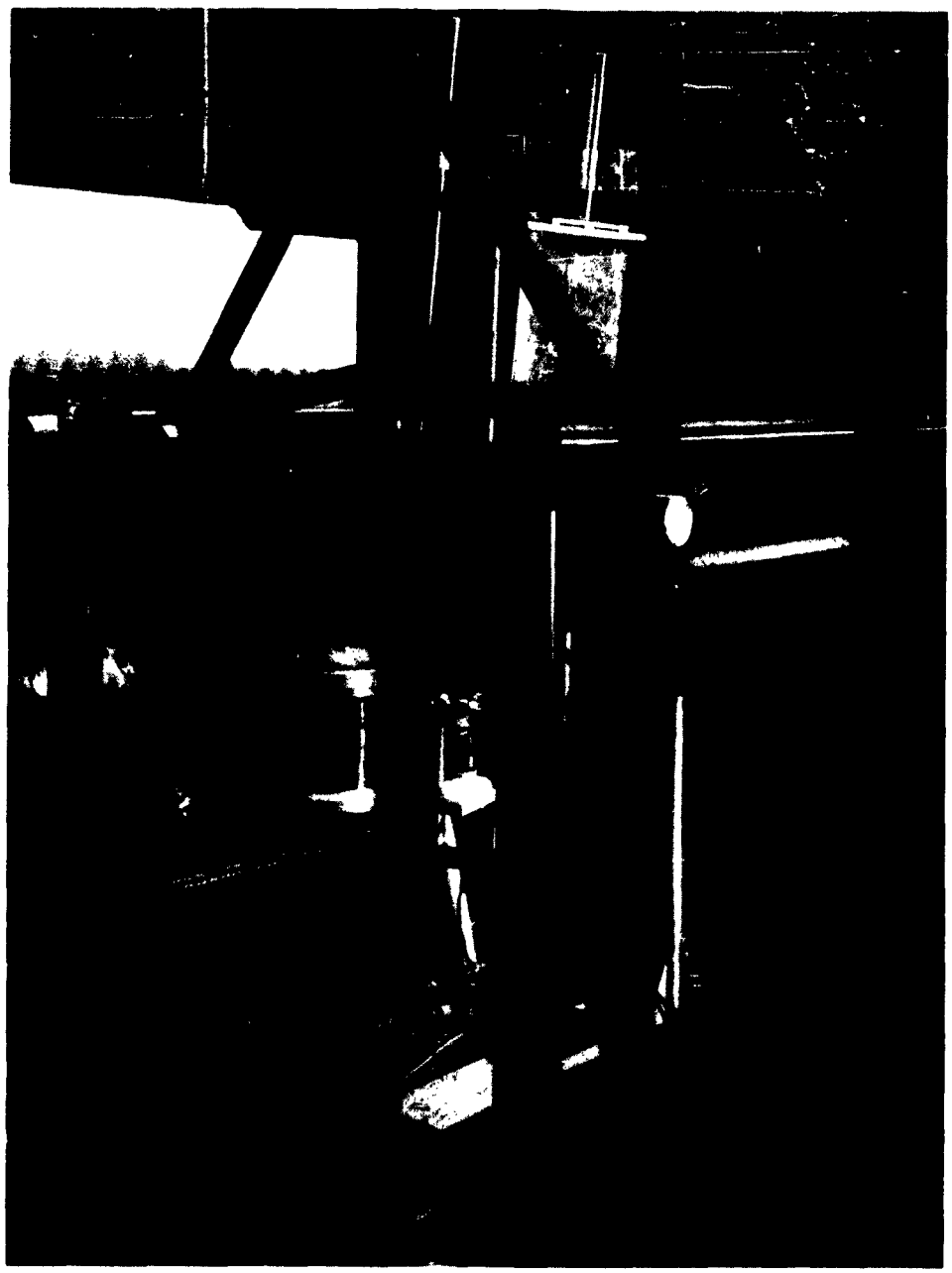

Figure 31

Partial View of Thermal Gradient Instrument.

NON-DESTRUCTIVE TESTING, INSPECTION - PYROLYTIC GRAPHITE

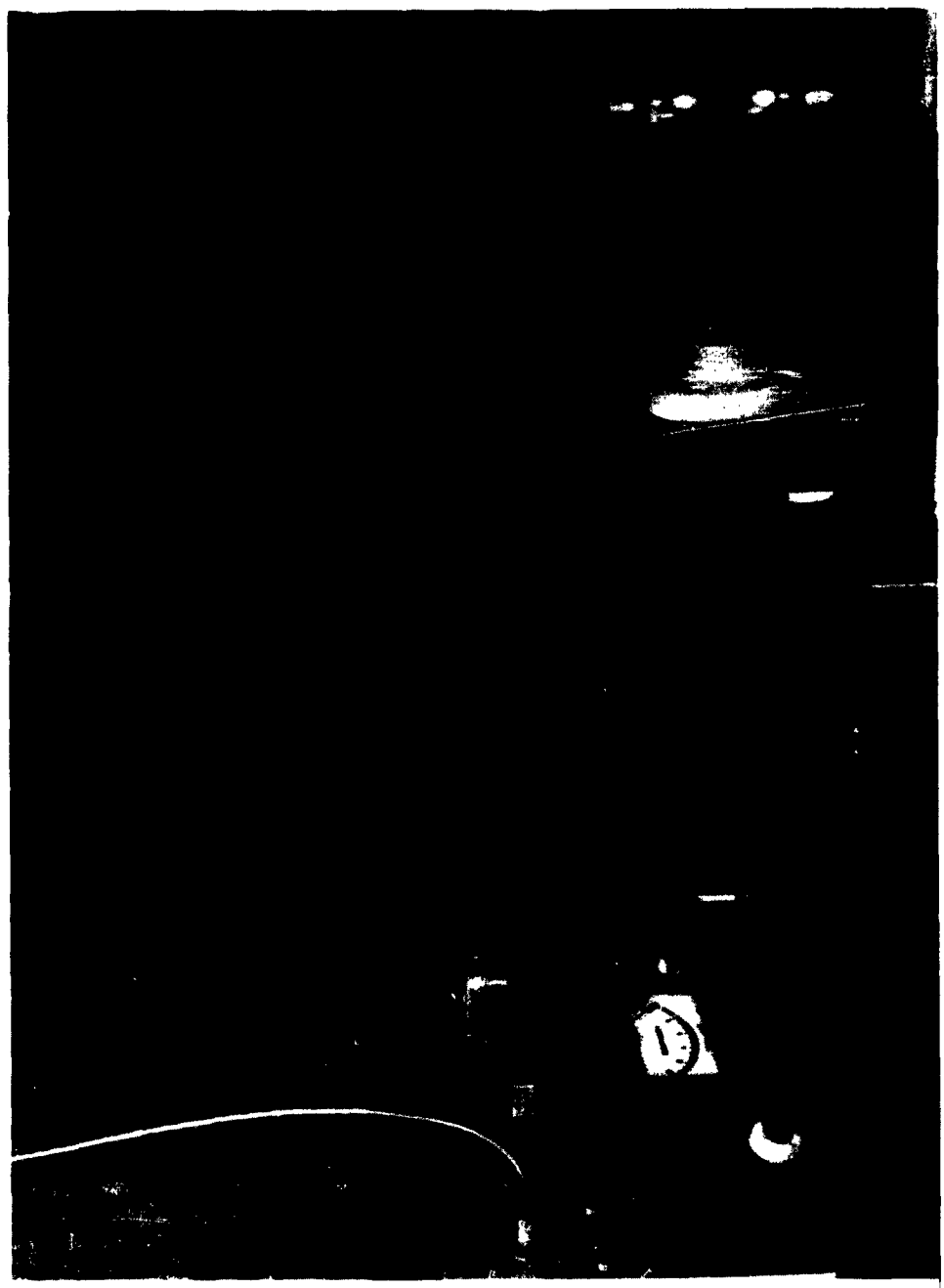

Figure 32

View of I. R. Lamp and Microampere Controls.

NON-DESTRUCTIVE TESTING, INSPECTION - PYROLYTIC GRAPHITE

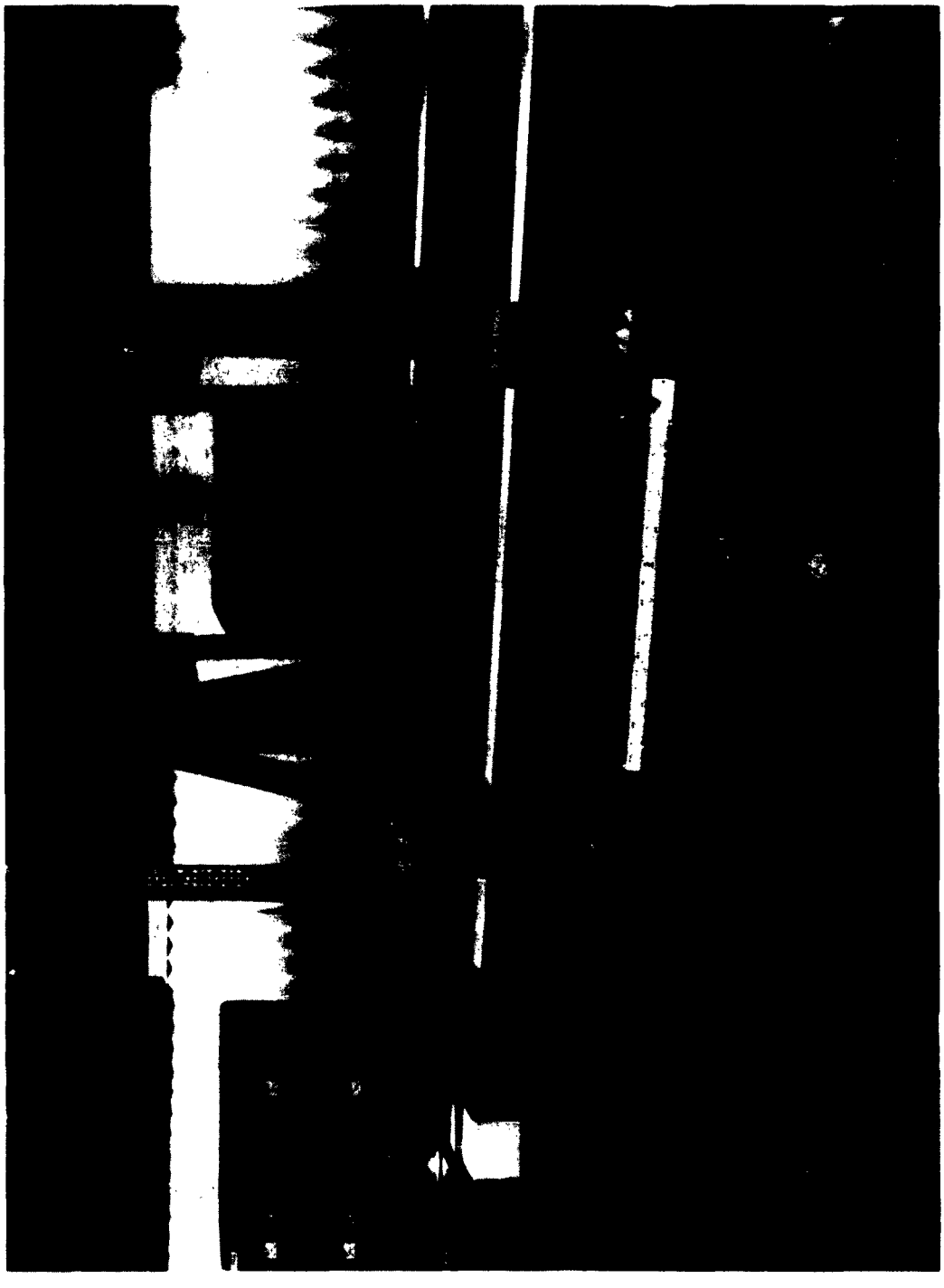

Figure 33
Thermal Gradient Equipment. Note Trace Recorder in Console.

NON-DESTRUCTIVE TESTING, INSPECTION - PYROLYTIC GRAPHITE

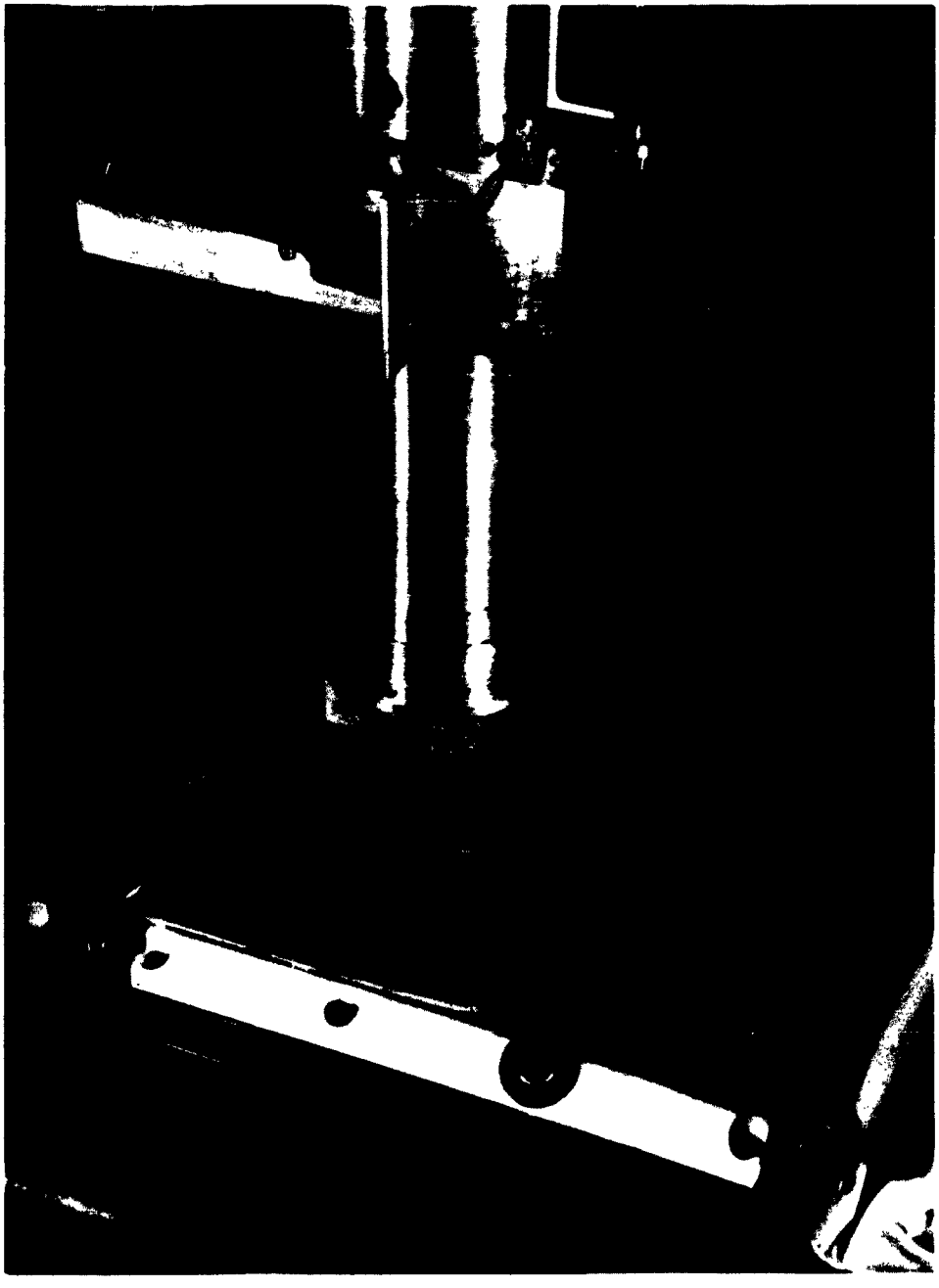

Figure 34

View of Test Sample and Probe in Thermal Gradient Apparatus.

NON-DESTRUCTIVE TESTING, INSPECTION - PYROLYTIC GRAPHITE

5.4.7 Miscellaneous - During the initial phases of the program it was of interest to accumulate extremely detailed information on vendors' shipments. Such information appeared necessary in evaluation of material quality and uniformity as related to the manufacturers' production variables. An idea of the completeness of the details recorded during this early stage may be gathered by an examination of the characteristics studied on representative specimens. These subjects are shown below.

1. Piece Idendification
2. Vendors' Run Number
3. Specimen Configuration
4. Type of Gas
5. Gas Pressure
6. Deposition Temperature
7. Rate of Deposition
8. Rate of Cooling
9. Minimum and Maximum Thickness
10. Area of Specimen
11. Radius of Surface Inch (Bow)
12. Surface Appearance - Mandrel
13. Surface Appearance - Deposition
14. Density - Vendor Analysis
15. Density - LMSC
16. Microstructure
17. X-Ray
18. Ultrasonic
19. Eddy-Current
20. End Use

There was some expectation that correlation of production variables with the non-destructive results would lead to improved material. It appears that some success in this direction was achieved, though admittedly not due entirely to these efforts, as evident by the more uniform and higher quality material that vendors furnished as production became better controlled. This condition was particularly true towards the expiration of the program.

6. CONCLUSIONS:

This investigation disclosed the effectiveness of non-destructive testing of pyrolytic graphite. It seems reasonable to conclude that such methods are entirely reliable for determination of surface discontinuities, internal flaws, and stresses.

Some further technique development in determining parallelism of layer planes is required. The Eddy-current method presently shows the most promise in this direction. However, the use of thermal gradient instruments may prove equally applicable.

NON-DESTRUCTIVE TESTING, INSPECTION - PYROLYTIC GRAPHITE

Perhaps the most objectionable characteristic found, particularly in early production specimens in pyrolytic graphite, was the evidence of internal stresses within the material. The use of X-ray Stress analyzer methods were most useful in locating these stresses. Analytical calculations illustrated the accuracy and reliability of such methods repeatedly.

It is felt that a great deal of basic information on both test methods and on the material itself was obtained during this investigation. The classified, experimental nature of many tests precluded recital in this report. However, with this foundation of fundamental non-destructive testing having been prepared, it seems reasonable to assume that future programs on pyrolytic graphite will be aided by the work.

NON-DESTRUCTIVE TESTING, INSPECTION - PYROLYTIC GRAPHITE

APPENDIX A

Photomicrographs	- Figures 1 through 7
Microstructure Classification	- Table 1
Microstructure Classification	- Figures 8, 9 and 10
Surface Photographs of Typical Specimens	- Figures 11, 12 and 13

NON-DESTRUCTIVE TESTING, INSPECTION - PYROLYTIC GRAPHITE

Figure 1A

Figure 1B

Figure 1

Sound Structures (50X)

NON-DESTRUCTIVE TESTING, INSPECTION - PYROLYTIC GRAPHITE

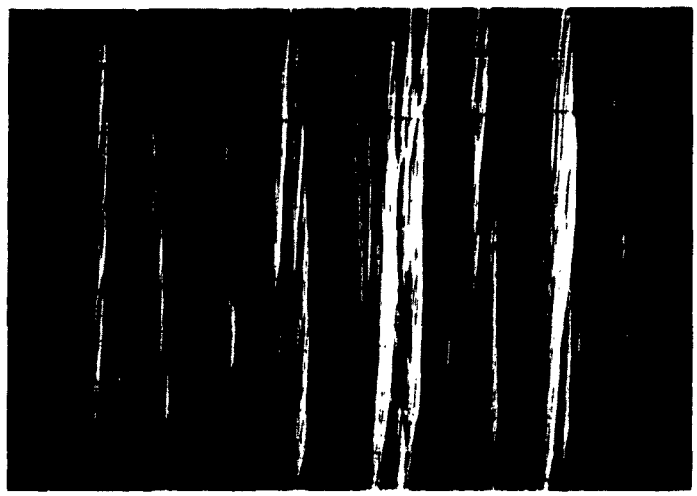

Figure 2A

Figure 2B

Figure 2
Unsound Structures (50X)
A. Laminations - B. Inclusions

NON-DESTRUCTIVE TESTING, INSPECTION - PYROLYTIC GRAPHITE

Figure 3
Abnormally Large Cone - Sound Otherwise (50X)

Figure 4
Good Structure with Slight Laminating Band (50X)

NON-DESTRUCTIVE TESTING, INSPECTION - PYROLYTIC GRAPHITE

Figure 5

Coarse Deposition Structure (800X)

NON-DESTRUCTIVE TESTING, INSPECTION - PYROLYTIC GRAPHITE

Figure 6

Fine Deposition Structure (800X)

NON-DESTRUCTIVE TESTING, INSPECTION - PYROLYTIC GRAPHITE

Figure 7

Deposition Surface Nodules (200X)

NON-DESTRUCTIVE TESTING, INSPECTION - PYROLYTIC GRAPHITE

Table 1

PYROGRAPHITE MICROSTRUCTURE CLASSIFICATION (Raytheon)

A. Primary Grain: Straight
   1. Coarse
   2. Medium
   3. Fine

B. Primary Grain: Curved
   1. Coarse
   2. Medium
   3. Fine (example not known)

C. Secondary: Straight
   1. Coarse (example now known)
   2. Medium
   3. Fine

D. Secondary: Curved
   1. Coarse
   2. Medium
   3. Fine

E. Intra-Layer: Straight
   1. Coarse
   2. Medium
   3. Fine

F. Intra-Layer: Curved
   1. Coarse
   2. Medium
   3. Fine

NON-DESTRUCTIVE TESTING, INSPECTION - PYROLYTIC GRAPHITE

Figure 8
Pyrographite Microstructure Classification,
100X Polarized Light, 15° From Extinction.

NON-DESTRUCTIVE TESTING, INSPECTION - PYROLYTIC GRAPHITE

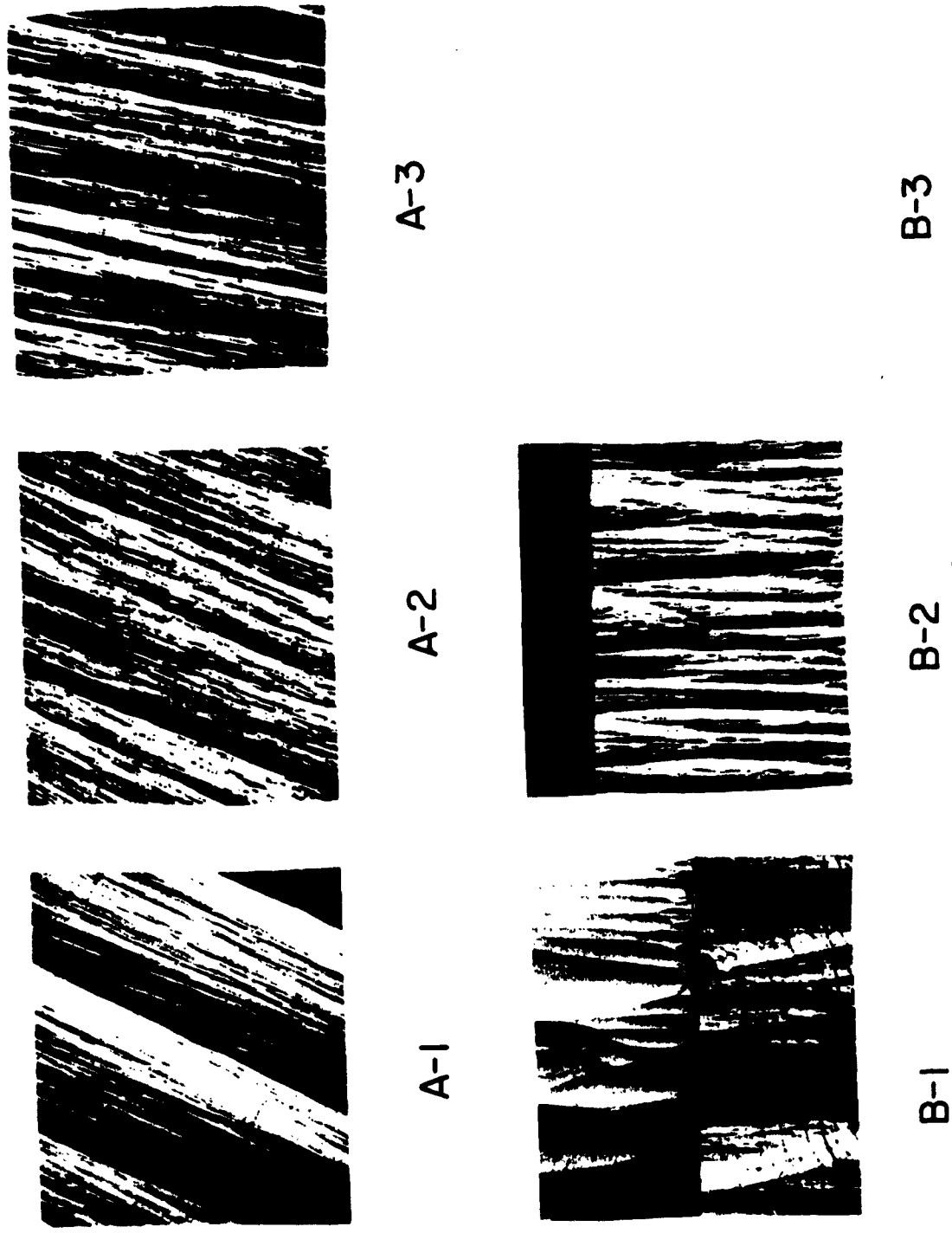

Figure 9
Pyrographite Microstructure Classification,
100X Polarized Light, 15° From Extinction.

NON-DESTRUCTIVE TESTING, INSPECTION - PYROLYTIC GRAPHITE

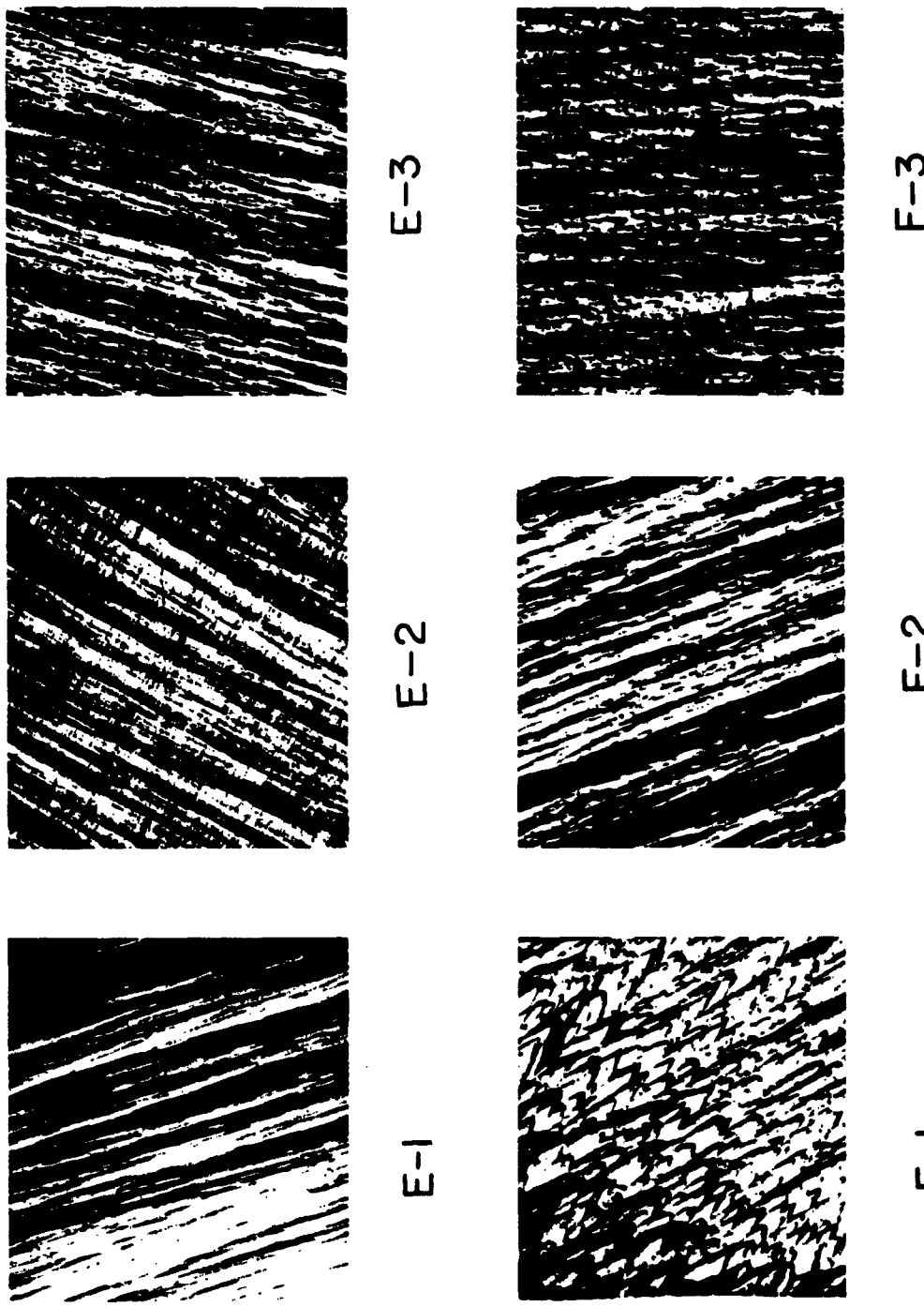

Figure 10
Pyrographite Microstructure Classification,
100X Polarized Light, 15° From Extinction.

NON-DESTRUCTIVE TESTING, INSPECTION - PYROLYTIC GRAPHITE

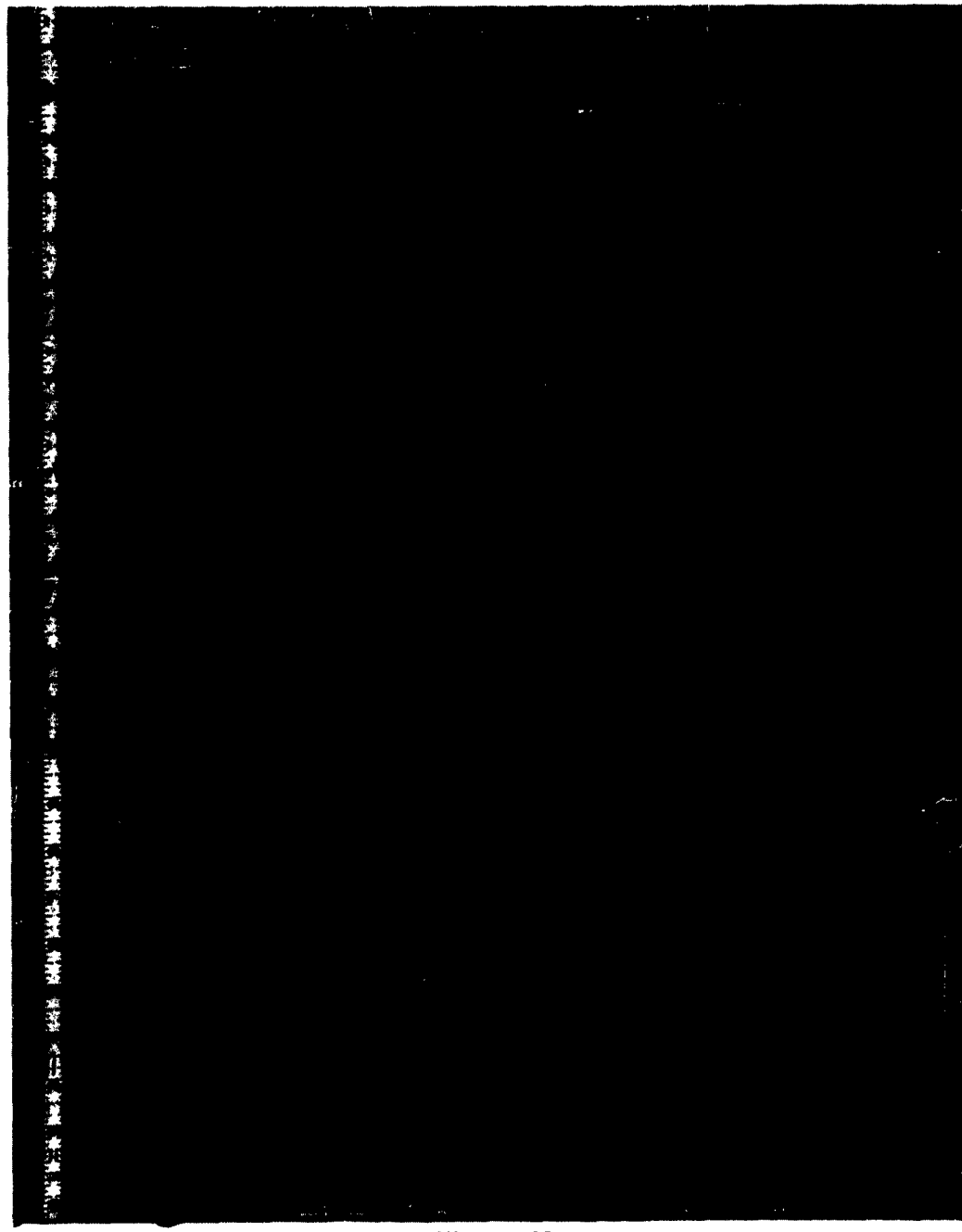

Figure 11

Deposition Surface

NON-DESTRUCTIVE TESTING, INSPECTION - PYROLYTIC GRAPHITE

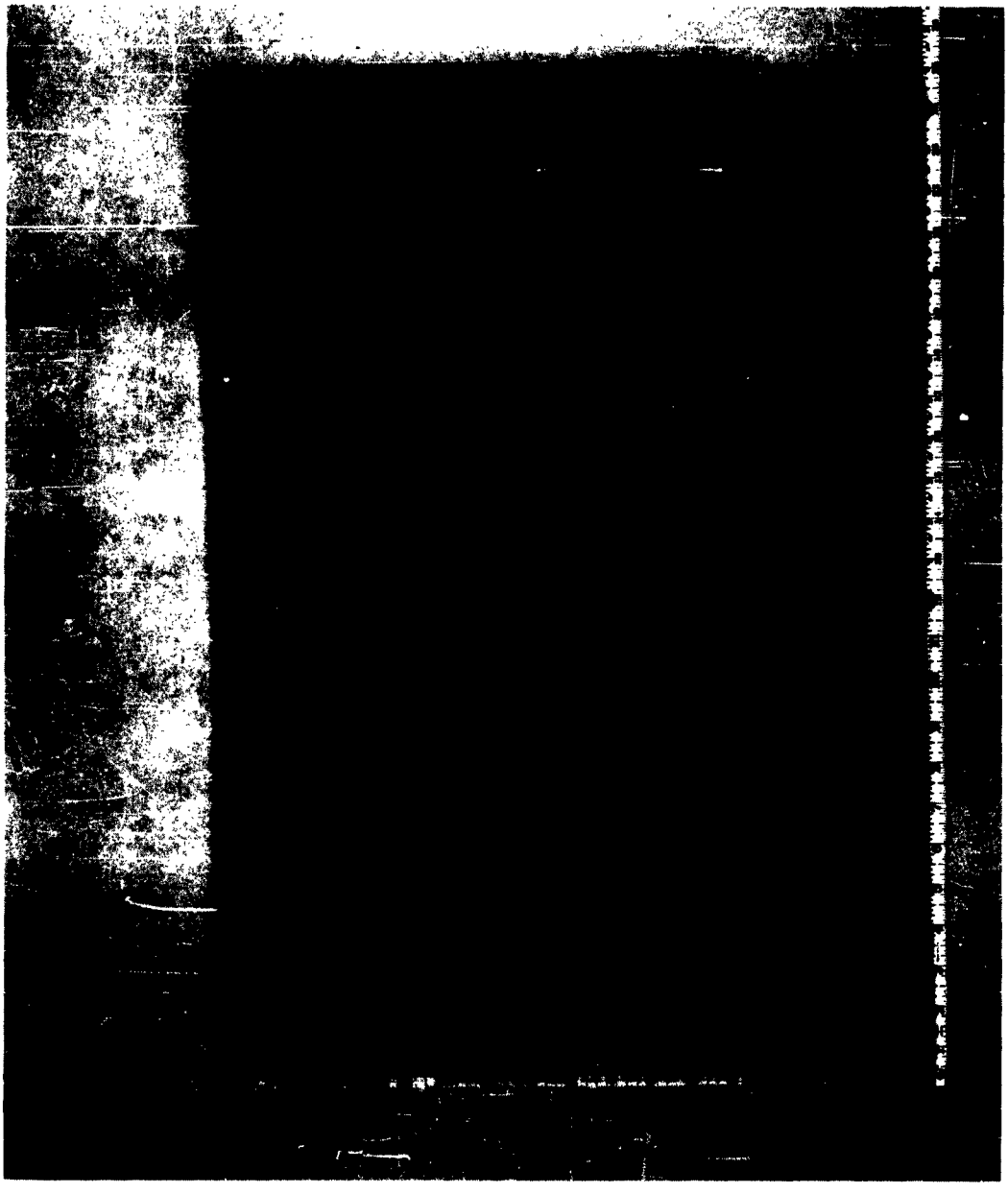

Figure 11A

Mandrel Surface

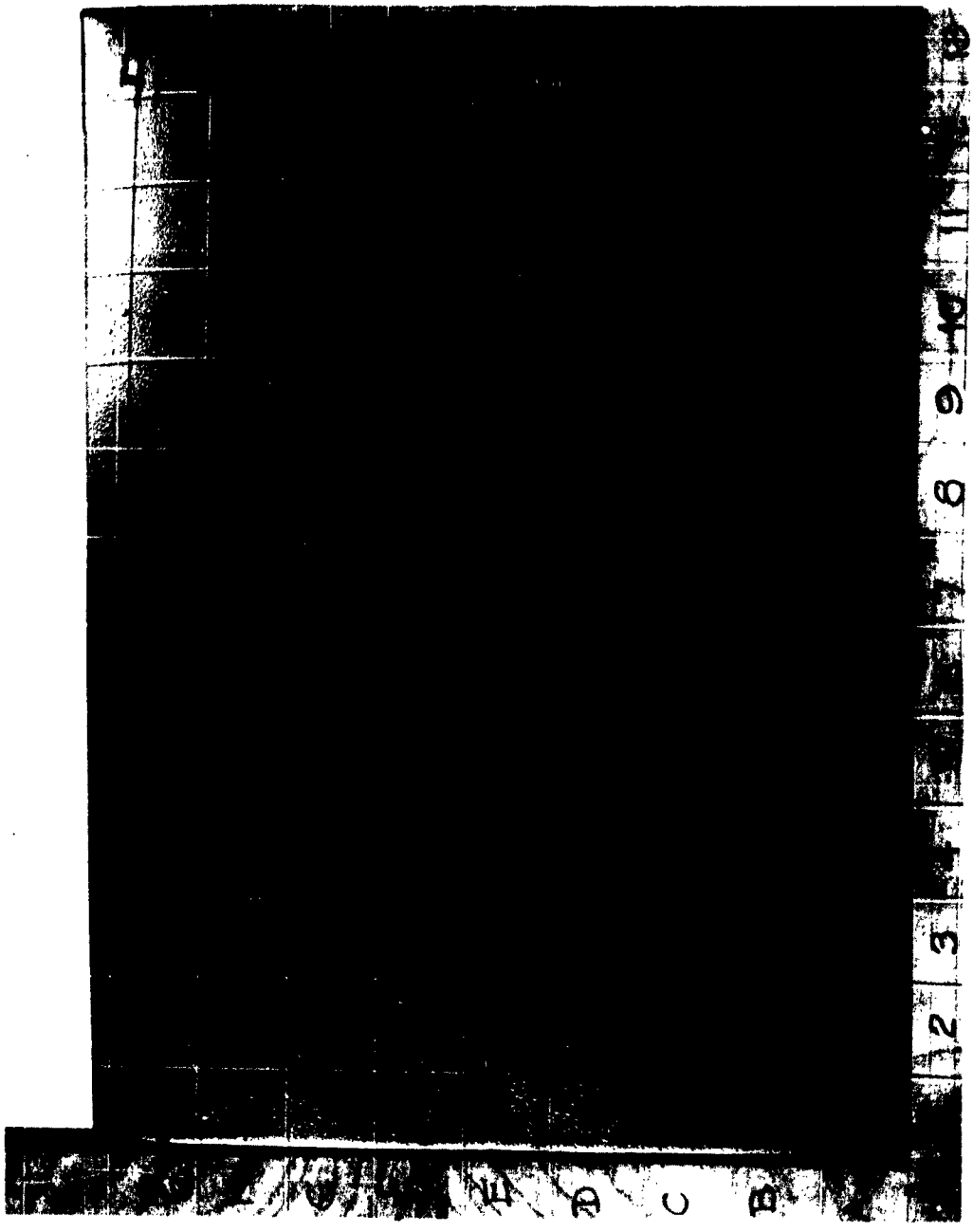

Figure 12

Deposition Surface

NON-DESTRUCTIVE TESTING, INSPECTION - PYROLYTIC GRAPHITE

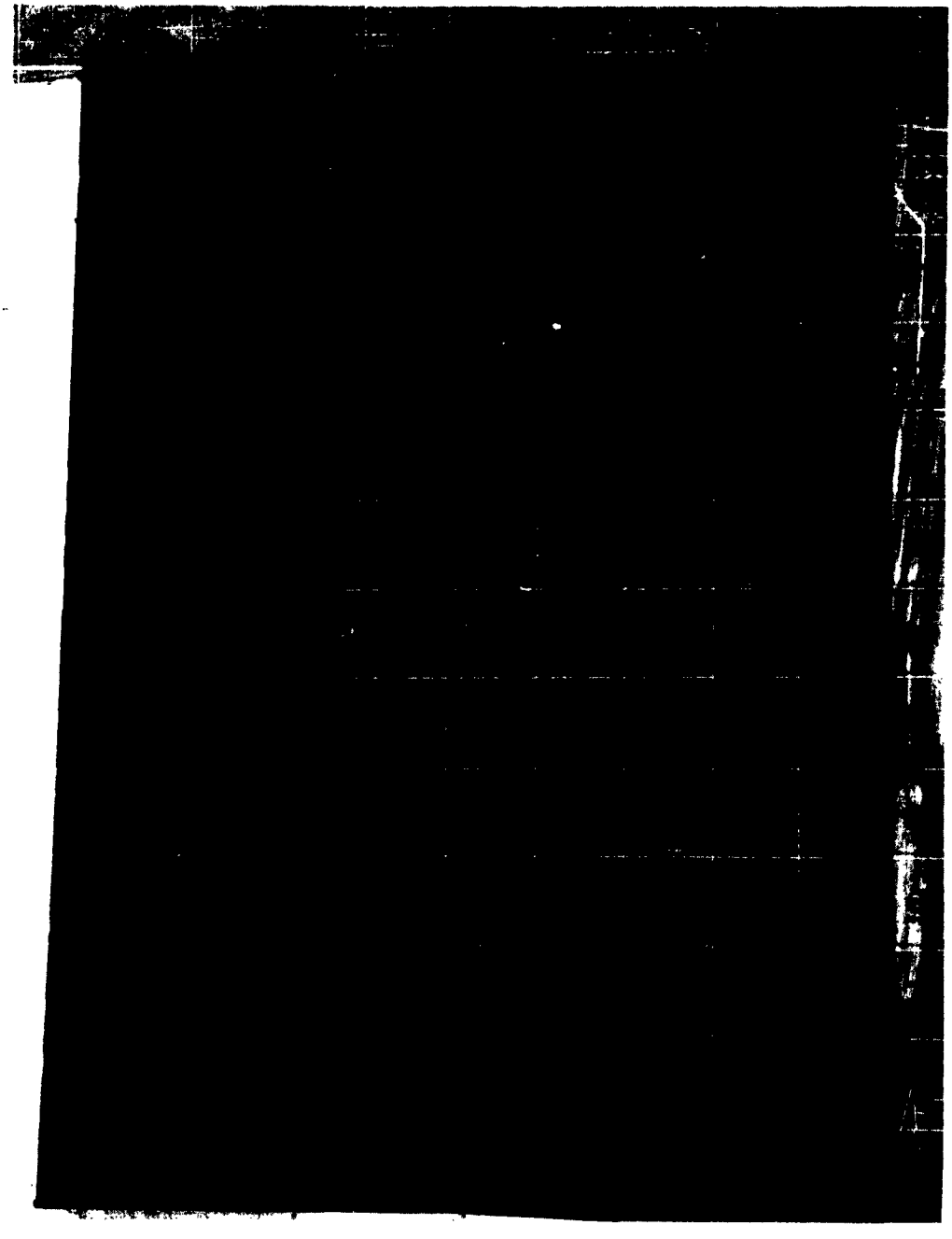

Figure 12A

Mandrel Surface

NON-DESTRUCTIVE TESTING, INSPECTION - PYROLYTIC GRAPHITE

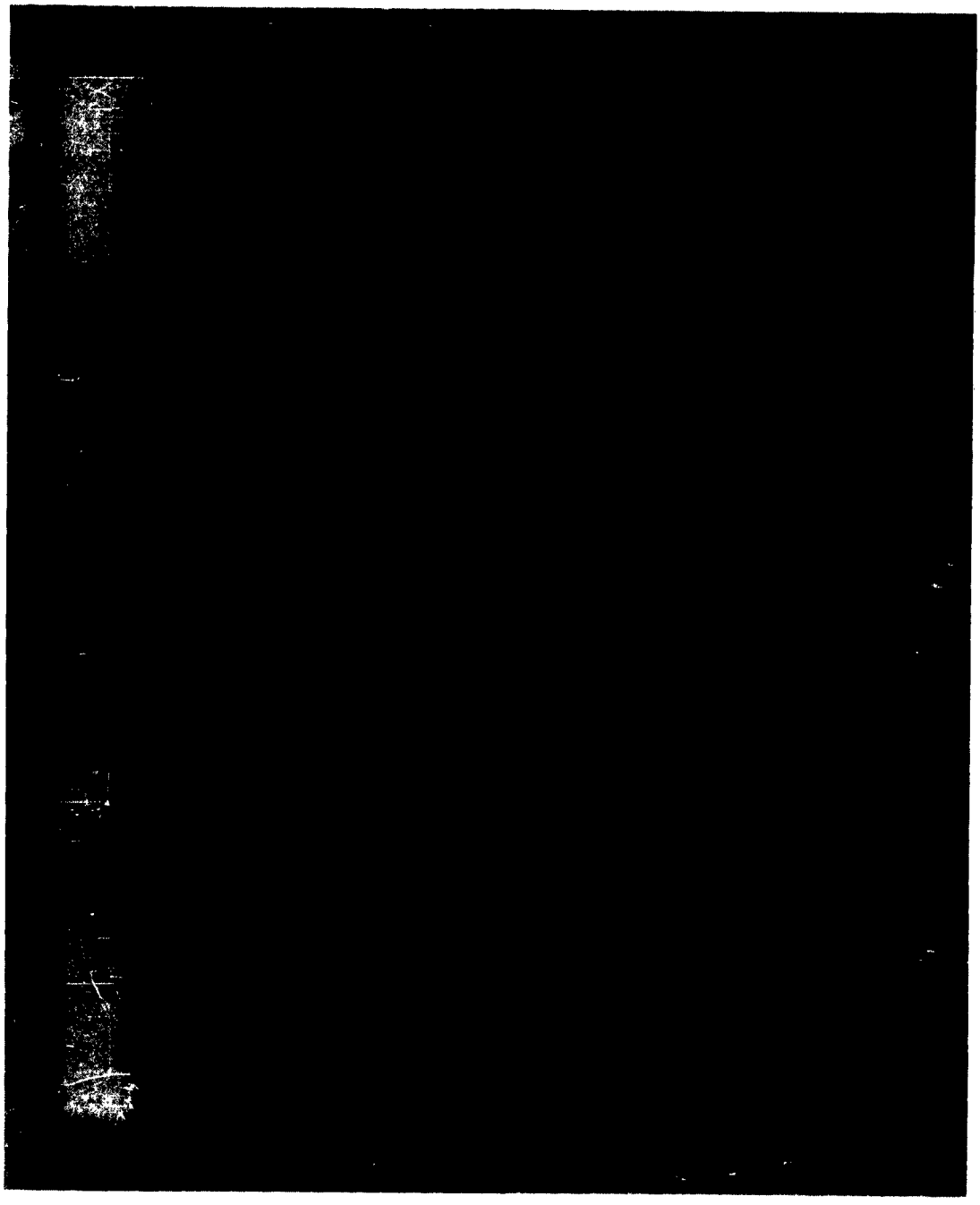

Figure 13
Deposition Surface
Large Amounts of Abnormal Nodules

NON-DESTRUCTIVE TESTING, INSPECTION - PYROLYTIC GRAPHITE

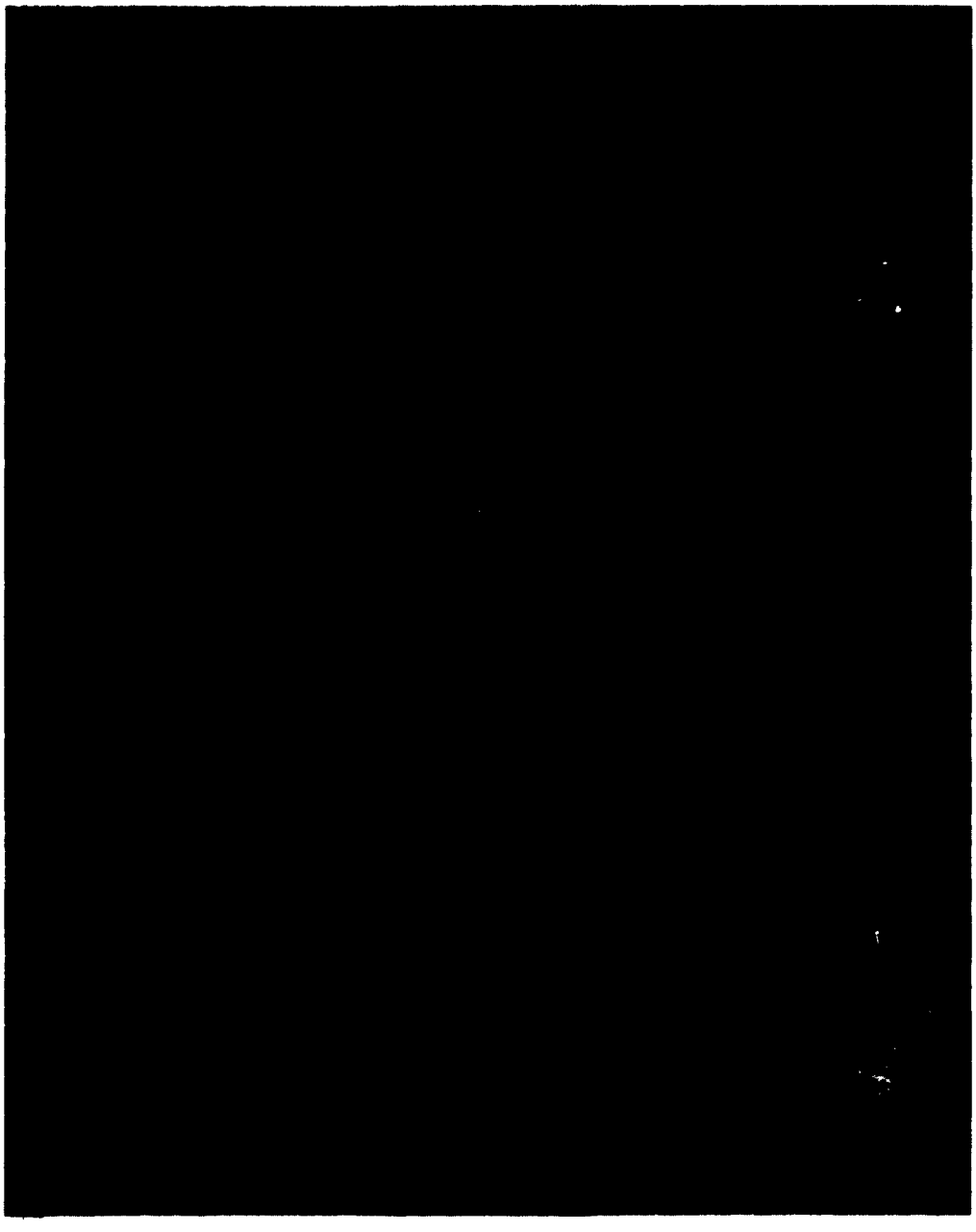

Figure 13A

Mandrel Surface - Sooty Condition

APPENDIX B

Mathematical Methods for Basic Computations Related to Stress Analyses by X-Ray

(Information furnished by R. Parker, Organization 81-41)

DRAWING 2.

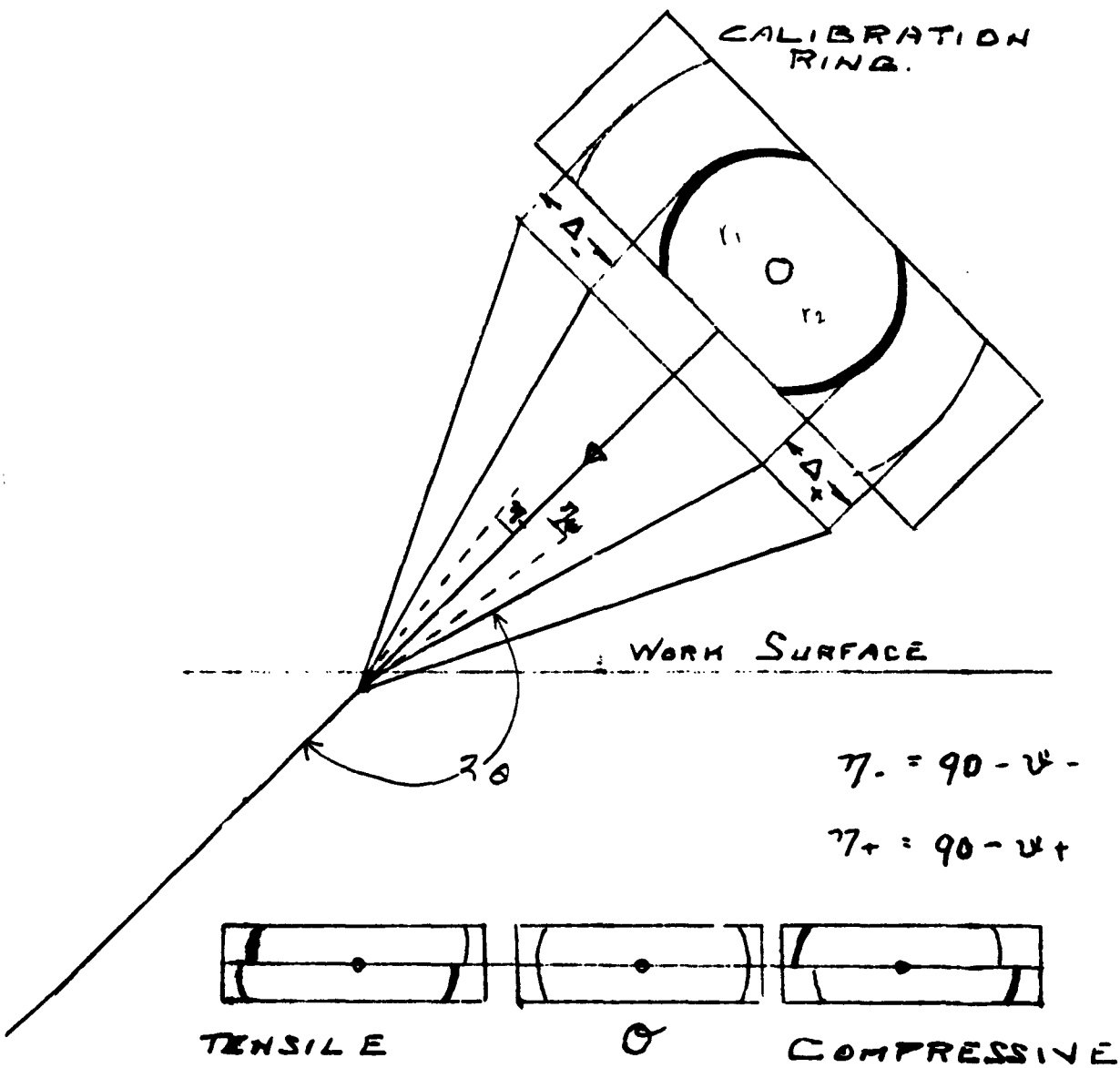

$\eta_- = 90 - \psi_-$

$\eta_+ = 90 - \psi_+$

FIGURE 1.

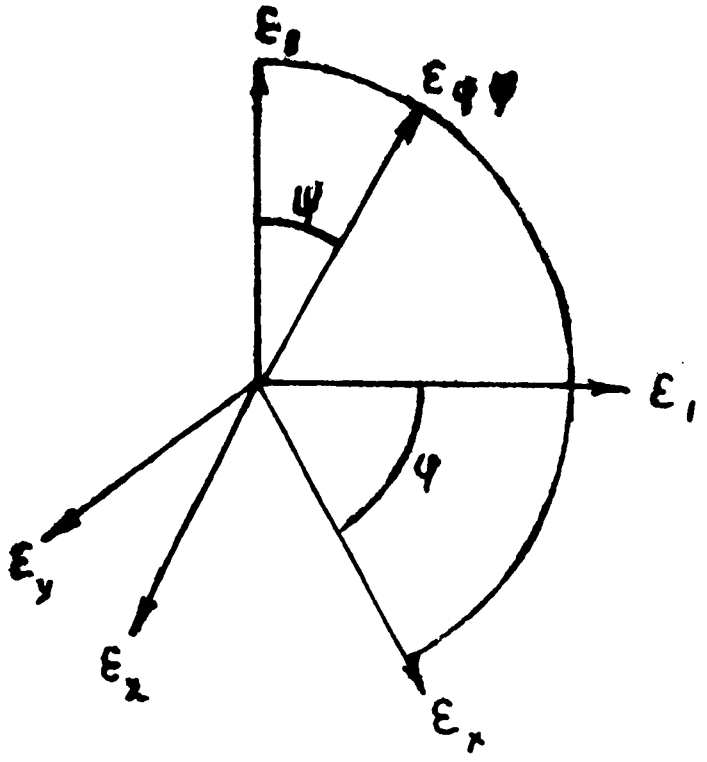

FIGURE 3.

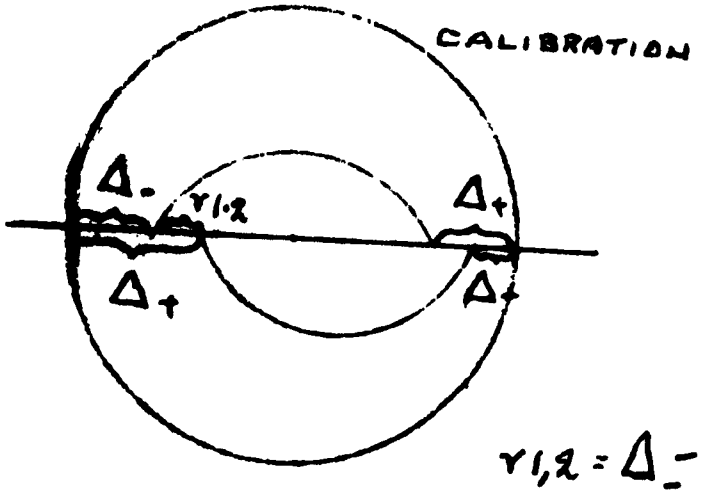

$\gamma_{1,2} = \Delta_- - \Delta_+ > 0$ TENSION STRESS

$\gamma_{1,2} = \Delta_- - \Delta_+ < 0$ COMPRESSION STRESS

The X-Ray Stress Analyzer

is an easily movable apparatus which is applicable everywhere because of its simple and sturdy construction. All geometric data are preadjusted as constants of the apparatus so that only line displacement is to be compared. Simply by multiplication of the line displacement and material constant the desired evaluation of the stress can be obtained.

1. Basic Principles of the Method

As in other determination of stresses, the radiographic stress indication is an expansion determination. In this radiographic method, the atomic distances are the gauges. The relation of both factors, expansion and stress, is formulated in Hooke's Law. On the other hand, Bragg's Law provides the grating constant at a given wave length, and, therefore, the expansion is compared to the stress-free status. Thus the compilation of both equations--with given wave length and misalignment--furnishes the conclusion of the stress.

Principally, only the back reflection range applies, and, therefore, a wave length of x-rays is necessary which forms an intensity- strong Debye-Scherrer ring. For that reason, monochromatic radiation is used which means that a constant family of plane surfaces of the crystal-lattice plane is used for the determination of stress, and not--as in mechanical determination--a mean value.

Without going into the derivation of the equations at this stage, (see end of text) the following equations lead to the final formula:

According to the law of elasticity:

$$(1)\quad \varepsilon_x E = \sigma_x - \nu(\sigma_y + \sigma_\perp)$$
$$\varepsilon_y E = \sigma_y - \nu(\sigma_x + \sigma_\perp)$$
$$\varepsilon_\perp E = \sigma - \nu(\sigma_x + \sigma_y)$$

(Explanation of letters for these and the follow-equations at the end of the text.)

For the difference of two expansions with the angles φ (in the x y - plane) and divergent angles ψ (see drawing 1), the following applies:

$$(2a)\quad E(\varepsilon_{\varphi,\psi_1} - \varepsilon_{\varphi,\psi_2}) = (\sigma_x - \sigma_\perp)(1+\nu)\{\sin^2\psi_1 - \sin^2\psi_2\}$$

Therefore:

$$\psi_1 = \psi_0 + \eta$$
$$\psi_2 = \psi_0 - \eta$$
$$\psi_0 = 45^\circ$$

If ψ_0 is the single entrance, then:

$$(2b)\quad E(\varepsilon_{\varphi,\psi_1} - \varepsilon_{\varphi,\psi_2}) = (\sigma_x - \sigma_\perp)\sin 2\eta_0(1+\nu)$$

As the expansion is reflected in a change of the lattice plane distance, the following applies:

$$(3)\quad \varepsilon_{\varphi,\psi} = \frac{d_{\varphi\psi} - d_0}{d_0} = \frac{\Delta_{\varphi,\psi}}{d_0}$$

and $$\varepsilon_{\varphi,\psi_1} - \varepsilon_{\varphi,\psi_2} = \frac{d_{\varphi\psi} - d_{\varphi,\psi_2}}{d_0} = \frac{\Delta_{\varphi,\psi_1} - \Delta_{\varphi,\psi_2}}{d_0}$$

(4) $$\approx \frac{d_{\varphi,\psi_1} - d_{\varphi,\psi_2}}{d_{\varphi,\psi_2}} = \frac{\Delta d_{12}}{d}$$

because d, even in case of high stresses, seldom varies.

(5) Differentiating Bragg's equation: $n\lambda = 2d \sin\vartheta$, $2d\cos\eta$

we $\eta = \frac{\pi}{2} - \vartheta$

results in:

(6) $$\Delta d = \frac{n\lambda}{2} \frac{\sin\eta}{\cos^2\eta} \Delta\eta$$

according to drawing 2

(7) $$r = A\,tg\,(180° - 2\vartheta) = A\,tg\,2\eta$$

(8) $$\frac{\Delta r}{\Delta\eta} = A \frac{2}{\cos^2 2\eta}, \quad \Delta\eta = \frac{\Delta r}{2A} \cos^2 2\eta$$

(8) inserted in (6) results in:

$$\Delta d = \frac{n\lambda}{2} \frac{\sin\eta}{\cos^3\eta} \cos^2 2\eta \frac{\Delta r}{2A}$$

or

(9) $$\frac{1}{d} \frac{\Delta d}{\Delta r} = \frac{n\lambda}{2} \frac{\sin\eta}{\cos^3\eta} \cos^2 2\eta \frac{1}{2A} \frac{1}{d}$$

(5) inserted in (5) $$\frac{n\lambda}{2d} = \cos\eta;$$

inserted in (9) results in:

(9b) $$\frac{\Delta d}{d} = \frac{\sin\eta}{\cos^3\eta} \cos\eta \cos^2 2\eta \frac{\Delta r}{2A}$$

on the other hand (2b) and (4) show that:

(10) $$\varepsilon_{\varphi,\psi} - \varepsilon_{\varphi,\psi_2} = \frac{\Delta d_{12}}{d} = \frac{\sigma_\varphi - \sigma_\perp}{E} \sin 2\eta (1+\nu)$$

(10) and (9b) in an equation are:

$$\sigma_x - \sigma_\perp = \frac{E}{1+\nu}\,\frac{1}{2A}\,\frac{tg\,\eta\cos^2 2\eta}{\sin 2\eta}\,\Delta r_{12}$$

IF $\Delta r_{12} = r_1 - r_2 = \Delta_- - \Delta_+$

If

$\Delta_1 - \Delta_+ > 0$ — tensile stress

$\Delta_- - \Delta_+ < 0$ — compressive stress

see drawing 2

2. Discussion of the Method

The generally accepted equation:

(11) $$\sigma_x - \sigma_\perp = \frac{E}{1+\nu}\,\frac{1}{2A}\,\frac{tg\,\eta\cos^2 2\eta_0}{\sin 2\eta_0}\,\Delta r_{12}$$

points out the possibility as well as the limitations of the applicability of the method.

In order to obtain the stress σ_x in a predetermined direction X following the surface of the material, the stress $\sigma_\perp$ must be vertical to the surface 0, or at least very small compared with σ_x. This generally occurs at an ideal surface. As x-rays have the tendency to penetrate through the material, $\sigma_\perp$ may be subject to deviation which, in practice, is very small compared with σ_x, in which case it can be evaluated from the material construction.

If the distance A = material surface : film is known and operation is performed with a certain wave length (η is given) the formula is simplified to:

$$\sigma_x = K\,\Delta r_{12}.$$

If A = 50 mm, the following values apply:

For Fe at cobalt radiation $K\alpha_1$: K = 75.
$K\alpha_2$: K = 77.

at Chrom radiation $K\alpha_1$: K = 72.
$K\alpha_2$: K = 72.

For Al at Cobalt radiation $K\alpha_1$: K = 25.1
$K\alpha_2$ K = 25.4

at Chrom radiation $K\alpha_1$: K = 16.5
$K\alpha_2$: K = 17

Theoretically, it is easy to indicate that a discrepancy in distance of 0.5 mm causes an error in the stress evaluation of only 1%, furthermore, that an angular inaccuracy of $\pm$ 5° results in an error in the same range only. The line distances to be expected will be some tenths of mm's, where 1/10 mm equals about 7 kilos per mm^2 with iron. For accuracy between 1/10 and 1/20 mm, the exposure can be evaluated without difficulty with a rapid comparator, so that the error cannot exceed $\pm$ 11.023 lbs. permm^2. The percentage of the error is in reciprocal relation to the stress.

The following premises are, therefore, to be observed in discussion of the results:

A. Principally only <u>one</u> family of crystal-lattice plane surfaces of a crystallite quantity is used for evaluation.

B. The stress is evaluated directly on the surface.

C. At not too critical an evaluation, the accuracy is ± 5 kilos per mm^2 with iron and ± 4.41 lbs. per mm^2 with aluminum. Of course, precision may be increased by more accurate evaluation.

D. The stress is evaluated at a predetermined point on the surface.

E. Errors which are caused by aperture of the diaphragm and by inclined incidence of the bundle of x-rays in the diaphragm may be ignored.

It is mandatory that the actual material surface is prepared and not a rust or oxide film. Therefore, the material must be prepared superficially with a hydrochloric acid rich mixture.

Electrochemical pickling as preparation for radiographic determination of stresses with Erescope.

Apparatus:

1. Electrolyte of the following ingredients:
   2 parts hyperchloric acid (60%)
   7 parts ethyl alcohol (96%)
   1 part glycerin
2. Car battery (6 volts)
3. 1.5 mm^2 connecting wire
4. Nickel rod, 4 - 5 mm diameter, 200 mm long <u>one end insulated</u>.
5. Sterile cotton
6. Fuel alcohol

Wiring Circuit:

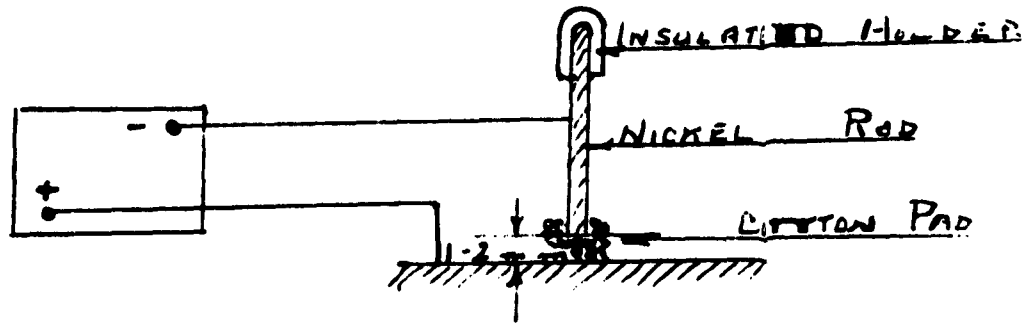

Procedure:

A. Point to be examined, about 20 mm^2, must be polished with corundum paper, avoiding deep grooves or scratches.

B. Wiring as per circuit.

C. Fasten cotton ball with rubber band on nickel rod.

D. Wet cotton with electrolyte.

E. Rub point to be examined 10 to 12 times for 6 to 7 seconds with electrolyte.

F. Remove residual electrolyte.
   1. Wipe with clean linen
   2. Rub three times with cotton which is wet with fuel alcohol, dry fast with hot dry air, no steam!

Precautions:

Prevent smoking and open fire! Hyperchloric acid, alcohol and gaseous hydrogen which develops at the electrolysis are inflammable!

Miscellaneous: The distance between point of contact and end of nickel rod is about 1 - 2 mm. Current intensity is 2 Amps. Use of controlling measuring instruments is not necessary. The effect of the electrochemical pickling may be determined with a small microscope (enlarging 40 to 50 times). The particles are readily visible whereas grooves are not visible.

3. Construction of the Back Reflection Camera and the Erescope.

The value Δr_{12}, i.e. the displacement of the lines, can be determined by different methods. The most obvious in: use of the line of a calibration medium. An added calibration medium, i.e. gold particles, indicates the calibration ring to which the relation of the misalignment may be evaluated (drawing 2). The disadvantage of this method is that it is difficult to apply the required thickness in an even layer, and longer exposure time is necessary.

Therefore, we recommend the following: One half of the film is covered while an exposure is taken where the projection of the shutter edge on the material is in the direction of the stress. After this exposure, the camera and covering plate are turned 180° so that the unexposed part of the film takes the place of the previous exposure.

The value $\Delta_{r_{12}}$ now is directly obtained by the line distance (drawing 3 shows the procedure). The uneven density is caused by the uneven absorption of the ray in the material (drawing 2).

The camera is adjusted by means of an adjusting device (picture 2 and 3) which determines angle and distance. The back reflection camera is attached to the tube shield which is mounted on a magnetic holding device and can be turned in any direction until the adjusting device indicates the proper position.

The tube is connected to the high voltage generator by means of a high voltage cable. A cooling unit cools the x-ray tube.

Detailed information on the technical data of the apparatus is given in the instruction book which accompanies the apparatus.

4. Applicability

Picture 5 shows the Erescope examining a vessel weld, and on picture 6 the inherent strain of a shrink ring gear is examined. Pictures 7, 8, and 9 show diagrams of different samples (the respective data are mentioned on a separate sheet).

At Cobalt radiation it is recommended to work with a filter for the Co K_β line because otherwise it might energize the iron. Usually Chromium radiation is applied, and then no filter is necessary, and exposure times range between 5 and 10 minutes.

Quick Comparator

This comparator was especially designed for fast evaluation of x-ray diagrams. Film, measuring scale and vernier are illuminated through a ground glass plate, whereby the length can be determined--and may be read through a magnifying glass--up to an accuracy of 1/10 mm. The magnifying glass enlarges three times. Experience has proved that this enlargement is best for x-ray exposures.

Explanation of Symbols

E = modulus of elasticity

ν = Poisson's ratio

η = Bragg's angle

α = reflection angle

λ = wave length

r = radius of Debye-Scherrer ring

A = distance between material surface : film

σ_x = direction of stresses

ε_x = expansions

d_x = distances of lattice surfaces

$\Delta_{+,-}$ = line displacement

Explanation of Pictures

No. 7 Diagrams of Iron
Cr-tube, exposure time 10 minutes

7a Strain $\Delta r = -0.25$ mm
$\sigma = -18$ Kg/mm²

7b Stress $\Delta r = 0.15$ mm
$\sigma = 11$ Kg/mm²

8 Diagrams of Steel
Co-tube with Fe-filter, exposure time 10 min.

8a Strain $\Delta r = 0.32$ mm
$\sigma = 24$ Kg/mm²

8b Stress $\Delta r = 0.15$ mm
$\sigma = 11$ Kg/mm²

9 Diagrams of Aluminum
Co-tube without filter, exposure time 10 min.

9a Strain $\Delta r = -0.2$ mm
$\sigma = -5$ Kg/mm²

9b Stress $\Delta r = 0.2$ mm
$\sigma = 5$ Kg/mm²

Note (for pictures 7 to 9)

These exposures are slightly overexposed for reproduction purposes; on the originals the differences are readily visible. For the above diagrams a slit diaphragm of 0.3 x 3 mm was used. Each back reflection camera for the Erescope is furnished with a circle diaphragm of 1 mm diameter and the slit diaphragm of 0.3 mm x 3 mm, which may be used alternatively.

Important Data for Radiographic Determination of Stresses

Radiation Used	λ [Å]	Specimen	Lattice Constant [A]	Effective Plane Surfaces	Modulus of Elasticity	γ_0	$K\left(\sigma = K\Delta r \left[\frac{K_g}{\Delta r \text{ in mm}}\right]\right)$
Cr-K_α	2.2850	α Fe	2.8610	(211)	8200-8300	11° 59-2/3'	71.6-72.6 ≈ 72
Co-K_α	1.7853	α Fe	2.8610	(310)	8200-8300	9° 22½'	74.6-75.6 ≈ 75
Cr K_α	2.2850	Al	4.0414	(222)	2700	11° 39'	23.7
Co-K_α	1.7853	Al	4.0414	(420)	2700	8° 58'	25.1
Cu-K_α	1.5374	Al	4.0414	(511) (333)	2700	8° 44½'	25.2
Cr-K_α	2.2850	Mg	3.203	(104) (014)	1900	13° 52-2/3'	15.79
Co-K_α	1.7853	Mg	3.203	(204) (024)	1900	19° 44'	12.78
Cu-K_α	1.15374	Mg	3.203	(124)	1900	19° 36'	12.3

The pressure of stress σ in kg/mm^2 are determined by the equation $\sigma = K\Delta_{\gamma/\alpha}$ in the line displacement $\Delta_{\gamma/\alpha}$

The deviation of this equation and the value of the constant K for various materials can be seen in the enclosed description.

Attention is drawn to the fact that= only Co-radiation is applicable for examination of Fe, Mg, or Al.